AN INTEGRATED MULTI-FUNCTIONAL MICROFLUIDIC DEVICE WITH PUMPING, PARTICLE SORTING, AND MIXING FUNCTIONS

A Thesis Submitted to the
College of Graduate and Postdoctoral Studies
In Partial Fulfillment of the Requirements
For the Degree of Master of Science
In the Department of Mechanical Engineering
University of Saskatchewan
Saskatoon

By

Yongqin Yang

PERMISSION TO USE

In presenting this thesis in partial fulfillment of the requirements for a Postgraduate degree from the University of Saskatchewan, I agree that the Libraries of this University may make it freely available for inspection. I further agree that permission for copying of this thesis in any manner, in whole or in part, for scholarly purposes may be granted by the professor or professors who supervised my thesis work or, in their absence, by the Head of the Department or the Dean of the College in which my thesis work was done. It is understood that any copying or publication or use of this thesis or parts thereof for financial gain shall not be allowed without my written permission. It is also understood that due recognition shall be given to me and to the University of Saskatchewan in any scholarly use which may be made of any material in my thesis.

Requests for permission to copy or to make other use of material in this thesis in whole or part should be addressed to:

Head of the Department of Mechanical Engineering
University of Saskatchewan
57 Campus Drive, Saskatoon, SK S7N 5A9, Canada

College of Graduate and Postdoctoral Studies
University of Saskatchewan
Room 116 Thorvaldson Building, 110 Science Place, Saskatoon, SK S7N 5C9, Canada

ABSTRACT

Currently, multiple functions are performed in microfluidic devices in a separate manner or in a manner that needs unnecessary transportation from one location, where one function is performed, to another, where another function is performed. There is a need to integrate these functions holistically to eliminate unnecessary steps and improve the performance of microfluidic system. This thesis was devoted to design and fabricate a microfluidic device that allows pumping, mixing, and particle separating functions to be performed simultaneously (or by eliminating any unnecessary transportation).

A design concept by introducing membranes into microfluidic devices was proposed based on Axiomatic design theory. Simulation was performed via the multi-physics software COMSOL and was validated with acceptable accuracy by experiments. The UV light lithography and soft lithography were employed to fabricate the device. A microfluidic device consisting of a main channel height of 50 μm, a main channel width of 30 μm, and membranes with a thickness of 10 μm, lengths of 300 μm and 200 μm was fabricated using Polydimethylsiloxane (PDMS).

The experiments were conducted to test the feasibility of the expected functions. The microbeads with diameters of 15 μm, 3 μm, and 200 nm were used to mimic the circulating tumor cells (CTC), normal blood cells and anti-cancer drugs, respectively. The experiment demonstrated the device effectiveness in terms of the mixing and particle separating functions. Unfortunately, the pumping function was not measured with the instrument available.

There are two main contributions. First, in the field of microfluidics, especially microfluidic device technology, the device is novel to the best of the author's knowledge. Existing devices perform more than one function but have a distinct time stamp to each of the functions and unnecessary transportations between each function unit. Second, in the field of biomedical engineering, this thesis provides a proof that the size- and deflection-based principle to separate two groups of particles, CTCs from the blood stream in this

case, is working. Subsequently, it is promising to further shape it to a practically viable device to separate CTCs from the blood stream.

ACKNOWLEDGEMENTS

What I have achieved from the wonderful experiences over the three-year study at the University of Saskatchewan is beyond any word. Firstly, I sincerely appreciate my research supervisor, Dr. Chris Zhang, for his professional guidance and continuous encouragements throughout this study. Without his guidance and critical comments on my work it is not possible for me to accomplish the thesis, which could be one of the milestones in my life. My gratitude also goes to his patience and kindness, which helps me get through all the critical moments in my study. I also would like to thank Anthony Tony (PhD candidate in Professor Zhang's group), Professor S-M Yang (Shanghai University), Professor Ki-Young Song (Beijing Institute of Technology), and Professor Tao Yue (Shanghai University) for their valuable suggestions on the design, fabrication, and computer simulation of the proposed micro-channel system. I also want to thank Alireza Farahinia (PhD candidate in Professor Zhang's group) for his careful proof-reading of this thesis. Further acknowledgements are extended to my advisory committee members, Professor Ike Oguocha and Professor Lifeng Zhang, for their constructive advice and suggestions from the very first AC meeting.

Special thanks go to Dr. Bing Zhang who is not only my research guider but also my sole mate. Thanks for his permission to use the facility to conduct my experiments at the Intelligent Energy-based Tumor Ablation Laboratory, Shanghai University and his patient guidance and assistance to help with the experiment set up. Without his patience and encouragement, it would not have been possible to complete the thesis. Besides, I also thank the staffs from the Biomedical Science and Technology Center and the research center of the company ZHONGXINQIHENG (cchip) in Suzhou, China for their advice and help in the fabrication of the multi-functional device.

Finally, I would like to thank my parents (Mrs. Shunqiong Chen and Mr. Bin Yang) and my pet Meimei and Huahua for their continuous encouragements and company, which helped me to persevere and complete my graduate program.

Table of Contents

List of Tables

List of Figures

List of Abbreviations

CTCs: Circulating tumor cells

PDMS: Polydimethylsiloxane

PMMA: Polymethyl methacrylate

PS: Polystyrene

Chapter 1: Introduction

1.1 Background and motivation

The past two decades have witnessed the development of miniaturization, which resulted in the study of microfluidics in analytical chemistry and life science [1]. Microfluidic devices can be developed to control and manipulate a tiny volume of fluid to flow in microscale or even nanoscale to fulfill various functions [2]. The application of microfluidics has attracted interests in various areas, such as micro-arrays, DNA sequencing, sample preparation and analysis, cell separation and detection, and environment monitoring [1, 3]. A complete microfluidic system includes functional units that operate on samples and fluids [4]. The functional units include valves, pumps, actuators, switches, sensors, dispensers, mixers, filters, separators, etc. [2]. Among these functional units, pumps and mixers are two of the most important ones [1, 5]. Separators are also a very common and necessary element for particle separation.

Conventionally, the functional units are designed as a separate unit. For performing a behavior that requires multiple functions, one needs to transport samples from unit A to unit B. If the sample is cell or tissue, this situation is far away from the *in vivo* reality. One can have several units put together or as proximate as possible on one platform to reduce this unnecessary transportation. This idea may alleviate the burden of transportation but still cannot eliminate the need of transportation. Due to this, multi-functions cannot be simultaneously and continuously performed, which deviates in-vivo situations. Besides, such an idea certainly leads that the device is bulky. There are also concerns that cells may be contaminated during the transportation from one unit to another for processing.

A new device concept that can integrate several functions into one body, an idea of aggregation of components say A, B, C into ABC and potentially embedding instructions for the flow of fluids is worthy of investigation. This is the motivation of this thesis. In particular, this thesis attempted to study the feasibility of such microfluidic devices. This thesis took three functions in microfluidic devices as a study vehicle, namely pumping,

particle separating, and particle mixing functions. This thesis also took the organ-on-a-chip [6] or “factory-on-a-chip” as a broader context for the device concept to be studied and developed.

1.2 Research question

The research question of this thesis was thus:
Is it possible to have a new device concept to allow several functions, particularly pumping, particle separating, and particle mixing functions, to be performed simultaneously and continuously with a potential to be applied to an organ-on-a-chip system?

1.3 Research objectives and scope

The first step in device design is the architecture of the device, which is the most important information of the device according to Bi *et al*. [7]. The architecture of a system is also called the DNA of a system [8].

The overall objective of this thesis was therefore to develop a new architecture of microfluidic devices that allow pumping, particle separating, and particle mixing functions to be performed simultaneously and continuously. To achieve this overall objective, the specific objectives were defined and are described as follows:

1. to design a microfluidic device for integration of the functions of pumping, particle sorting, and particle mixing, performed simultaneously with the possibility that the device being fabricated with the current micro-fabrication techniques.
2. to compare the lithography-based approach and the 3D printing approach to fabrication of the designed device to explore the limit of the design and fabrication.
3. to build the test apparatus including the device as designed in objective 1 along with other instruments, and to test whether the expected functions of the device can be achieved along with its performance.

1.4 Organization of the thesis

The remaining part of this thesis consists of the following chapters. Chapter 2 will introduce further background information and discussion of related work relevant to the proposed research objectives to justify their need. In Chapter 3, a new architecture of the microfluidic device integrated with pumping, mixing and particle sorting functions will be presented. Chapter 4 presents a mathematical model of the membrane within the microfluidic device to predict its behavior to give confidence for prototyping of the multi-function microfluidic device. Chapter 5 presents device fabrication and assembly. Chapter 6 discusses the experiment on the prototype of the multi-function microfluidic device. Finally, Chapter 7 presents conclusions, contributions, and limitations of the work along with some thoughts for further research.

Chapter 2: Background and Literature Review

2.1 Introduction

The goal of this chapter is to provide further background information and to give a more comprehensive analysis of literature to justify the proposed objectives, as defined in Chapter 1. Section 2.2, Section 2.3, and Section 2.4 will discuss three functions in microfluidic devices, namely micropumps, micromixers and particle separators, respectively, as they were concerned by this thesis. Section 2.5 will discuss some multi-functional devices that integrate mixing and pumping functions on one platform in literature. In Section 2.6, the technological tools available for the fabrication of a microfluidic network will be discussed. Section 2.7 will discuss the design theory and methodology for guiding the design of the device in this thesis. Finally, the conclusion is shown in Section 2.8.

2.2 Micropump

As one of the most commonly used and the most crucial components among microfluidic elements, micropumps, fabricated by micro-electro-mechanical systems (MEMS) techniques [5], provide driving force for samples to flow through the channel in the system by manipulating a small volume of fluids [9]. According to Wang *et al*. [5], based on the working principle or mechanism, micropumps are classified into two types: mechanical and non-mechanical [10]. Mechanical micropumps have a physical actuator or mechanism to conduct pumping. On the contrary, non-mechanical micropumps perform the pumping function without physical actuators or mechanisms. Instead, it drives the fluid by transforming no-mechanical energy to kinetic energy to perform the pumping function [5, 11]. The commonly used micropumps are given in Fig. 2.1.

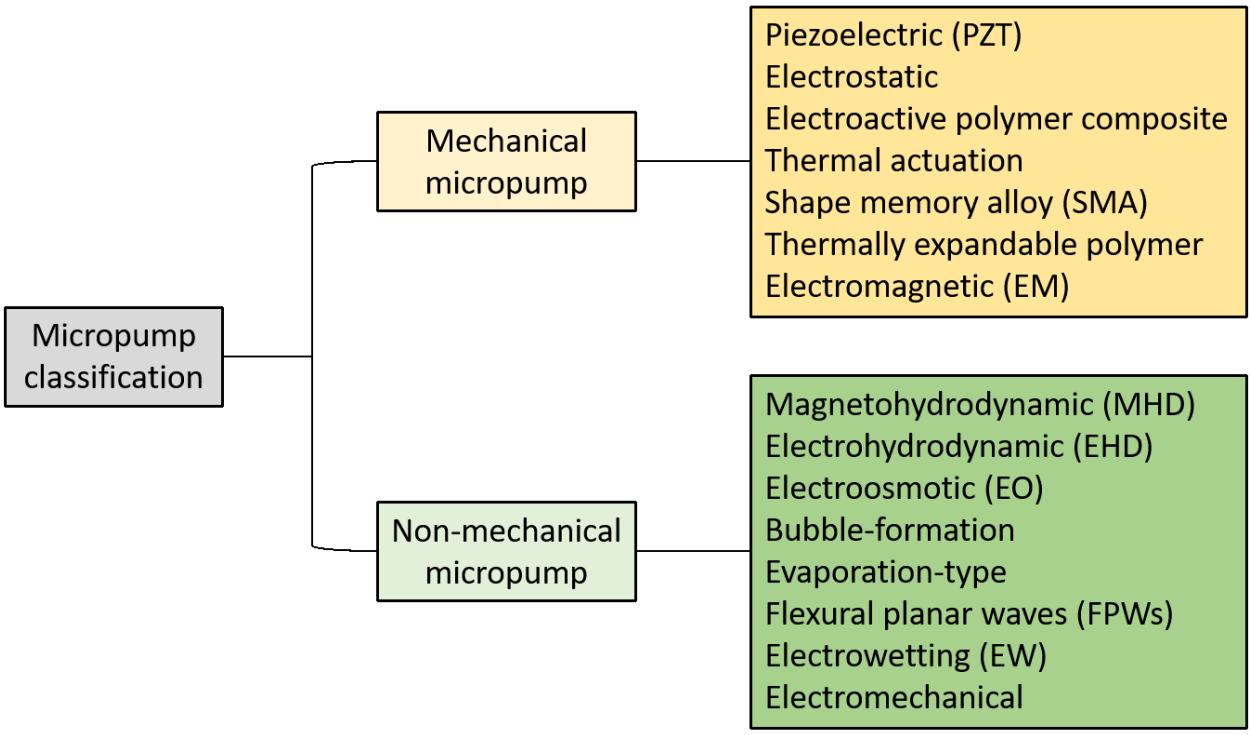

Fig. 2.1. Classification of micropumps [5, 11].

A hybrid polymer composite membrane was introduced by Said *et al*. [12] to act as an actuator, where the driving force was provided by the deflection of the membrane in EM micropumps. Fig. 2.2 is a scheme of the cross-sectional view of the EM actuator. The membrane was developed by mixing polydimethylsiloxane (PDMS) with neodymium magnetic particles (NdFeB). Planar coil wires with different layers were used to test the response of the membrane. Besides, a cylinder-shaped bulk NdFeB magnet with a diameter of 3 mm and a thickness of 2 mm was attached to the membrane to increase the magnetic force for membrane deflection. A schematic cross-sectional view of the EM actuator consists of EM coils, a permanent magnet and a deformable magnetic mechanical membrane. The deflection of the membrane is decided by the thickness of the membrane and the magnetic force between the EM coils and the permanent magnet [12].

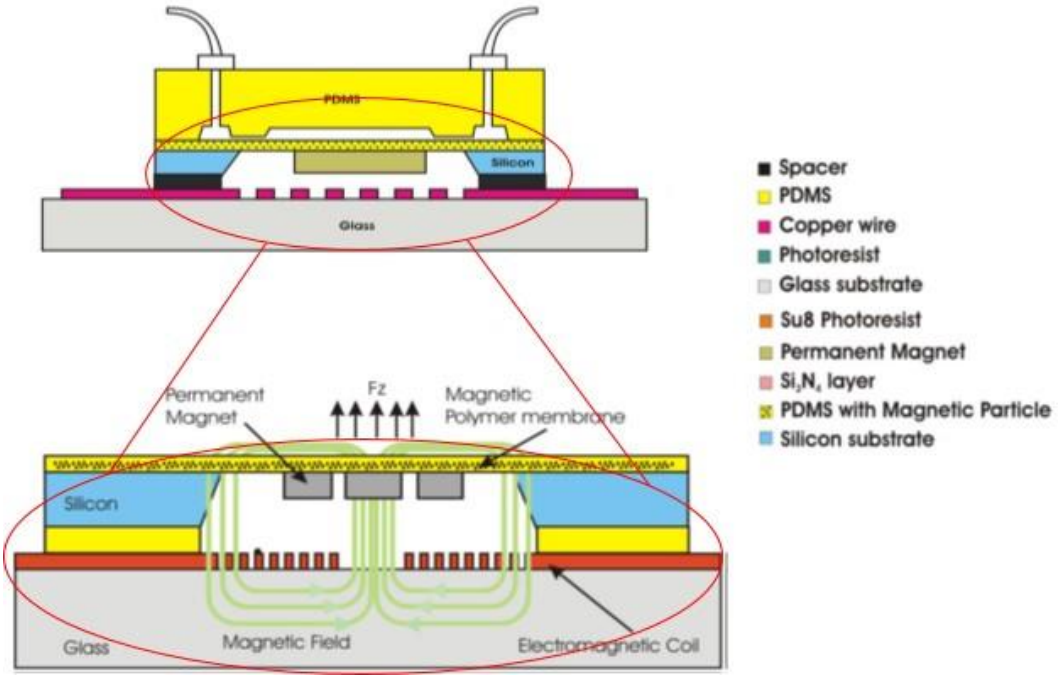

Fig. 2.2. A Schematic view of the electromagnetic micropump and the schematic cross-sectional view of the EM actuator [12].

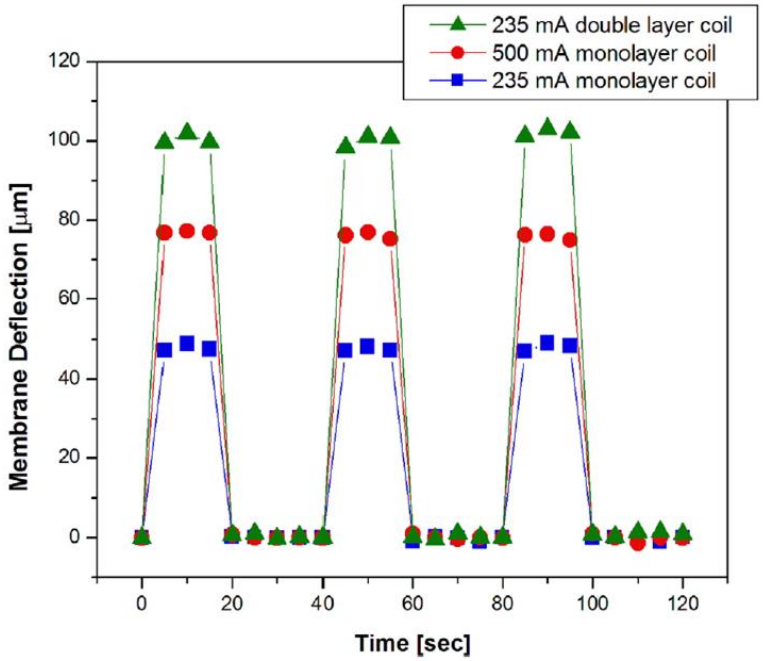

Fig. 2.3. The deflection of the membrane when applying a square input current signal [12].

Figure 2.3 shows the result of a deflection test of the EM actuator membrane [12]. The figure indicates that the membrane has a very high response to two types of coils. The membrane deflected immediately and reached the maximum deflection within 5 seconds as the circuit was turned on. The maximum deflection height was 106 μm [12].

2.3 Micromixer

Mixing in micro-channels may requires external turbulences and microstructures with a large surface to volume ratio. Moreover, the fluid velocity within the channel, the large Peclet number and the low Reynolds numbers (on the order of 1.0 and even smaller) lead to the laminar flow in microfluidic systems. This means that the mixing efficiency is very low because streams or samples will mix only by diffusion in the laminar flow condition [13, 14]. A long mixing channel and enough time for diffusion in a slow process can enhance the mixing function when the mixing function can only be performed by diffusion, but this may not be practical in applications [15, 16].

Generally, micromixers are divided into active and passive micromixers based on the mixing principles [1, 17, 18]. An active mixer requires external energy sources, such as electrical, magnetic, sound fields, and so on. A passive one requires complex channel geometries, with which to enhance the diffusion process and chaotic advection. The advantages and disadvantages of the active and passive micromixers are presented in Table 2.1 [13, 15].

Table 2.1. The advantages and disadvantages of active and passive micromixers [13].

	Active micromixers	Passive micromixers
Pros.	• Simple structure • Easy control	• Easy integration • Smaller size [16]
Cons.	• Difficult to integrate (external energy required)	• Complex fabrication process (long channels and time for molecular diffusion and chaotic advection)

In passive micromixers, the mixing mainly depends on molecular diffusion and chaotic advection. To improve mixing, the molecular diffusion needs to be increased by increasing the contact surface between different fluids and decreasing the diffusion path. Meanwhile, in active ones, the ratio between the time period of residence a fluid in the mixing chamber and the time period of disturbances to the fluid greatly influences the mixing efficiency. The fast flow leads to a short residence time, so the high disturbance frequency provided by external actuators is needed for good mixing [1].

Micromixers were applied to sample concentration [19, 20], chemical synthesis [21], chemical reactions [22], polymerization processes [23], extraction and purification processes [24], biological analysis processes [25], droplet/emulsion [26], and many other processes. For example, Jiang *et al*. [19] proposed a passive mixing approach by adopting a chaotic advection effect to obtain precise controls of both the composition and the shape of the immobilized gradient for the chemical concentrating process.

2.4 Particle separation

Cell or particle separation is a very crucial step in the biomedical field. For example, separating tumor cells from human blood samples is very important for cancer diagnosis [3]. Circulating tumor cells (CTCs) are cancer cells that circulate in the peripheral blood after being shed from the original or metastatic tumors [27]. The detection of CTCs can help with the early diagnosis of cancer. CTCs can be selected from blood or cell samples based on the size difference [28] and cell deformability [29], because the size of circulating tumor cells (CTCs) is normally much larger than that of normal blood cells and the CTCs are more rigid than normal blood cells. According to Allard *et a*l. [30] and Yi Dong *et al.* [31], the size of CTCs varies from 4 to 30 μm, and CTCs are usually 10 μm in diameter.

Cell separation has two types of methods: label-based and label-free method. The former one used an external magnetic field to select the labeled target cells [32-35]. The latter one sorts the target cells by applying forces, such as electrical forces which work with a

cell's charge and an electric firld, or a cell's polarizability [36-39], optical forces which manipulate the particles by a tightly focused laser beam [40-44], hydraulic forces which control cells via the altered fluidic resistance created by applying microstructures on a fluid path [45-47], and acoustical forces that apply sound waves [48-50]. The advantages and drawbacks of the commonly used label-free methods are listed in Table 2.2, respectively.

Table 2.2. Pros and cons of the commonly used label-free approaches [40].

	Pros.	Cons.
Dielectrophoresis (DEP)	Trapping cells without causing side effects to the cell and can sort cells with the size range of 5-10 μm compared with other electrical force methods [53]	Cell cannot be freely moved off the device and throughputs depend on the applied Alternating Current Dielectrophoresis (AC-DEP)
Optical force	Precise control of single cells	Low throughputs and potential damage to the cell
Acoustic force	Precise control of single cells, easily recovering the cell off the device, less invasive to cell than that of optical force	Low throughputs
Hydraulic force	Simple fabrication and application	Throughputs depend on the amount of trapping channels

The resistive pulse sensing (RPS) method introduced by Song *et al.* [51] is a novel sorting method based on RPS. Fig. 2.4 shows the structure of the device, which consists of one

main channel for sample solution, two focusing channels, two detecting channels, one pumping channel, and one collecting well. The two detecting channels are used to control particles moving at the center of the main channel so that the particles can pass through the sensing gate one at a time. The two detecting channels detect resistance changes when particles pass through the sensing gate. The pumping channel is used to pump the target particles into the collecting well [51]. Fig. 2.5 is a schematic diagram of the signal processing for the device of Fig. 2.4.

Song *et al.* [52] further proposed a novel microfluidic method to continually detect and count beads-labeled cells from a cell mixture without fluorescence labeling based on the size difference. Preira *et al.* [29] developed a perforated microfluidic device with pore sizes decreasing from the upstream to the downstream to passively separate the non-adherent cell population by deformability.

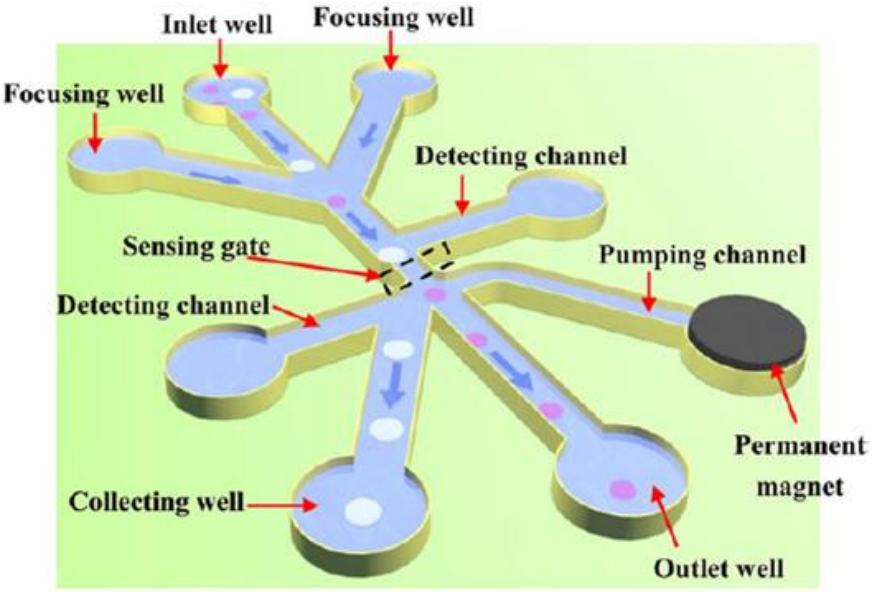

Fig. 2.4. A schematic diagram of the structure of the microfluidic device [51].

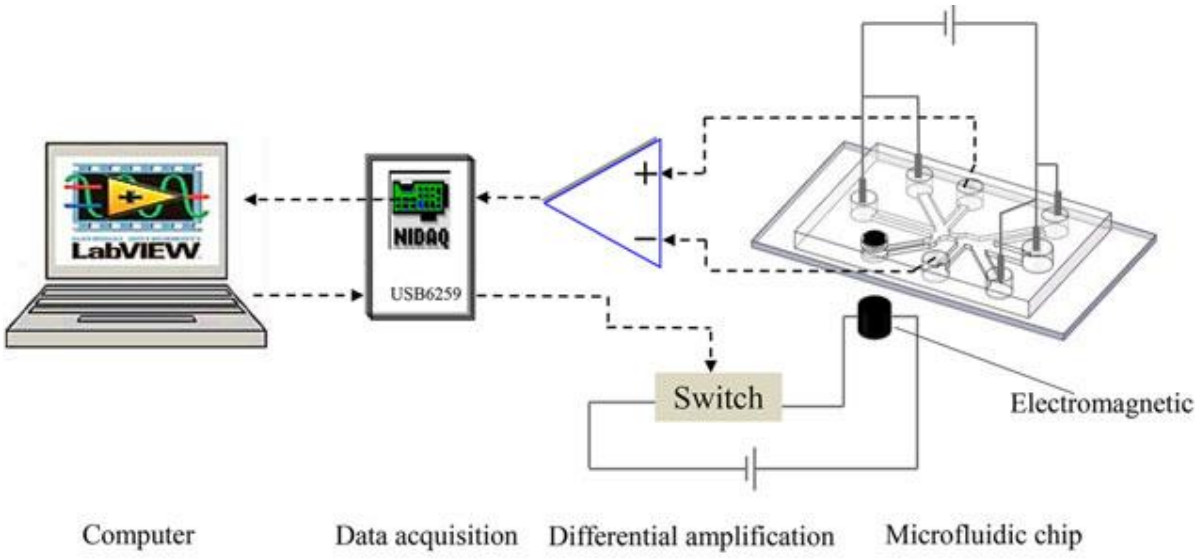

Fig. 2.5. A scheme of the system set up [51].

2.5 Multifunctional device with the mixing and pumping functions

Integrating pumping function with mixing function on one microfluidic device is a novel development. Fadl *et al.* [54] introduced a novel valve-less rectification micropump using Polydimethylsiloxane (PDMS) based on three different bifurcation configurations with the potential mixing function (combining the mixing function and the pumping function in micro scale). Kang *et al.* [55] presented the design and fabricated the magneto-hydrodynamic (MHD) micropump with the mixing function to obtain simultaneous mixing and pumping by coupling Lorentz force and the moving force of an electric charge in the electric field. Xiao *et al.* [56] also proposed a MHD micropump with the mixing function to get simultaneous mixing and pumping by judiciously applying different potentials to different electrode pairs to create Lorentz-force to direct the liquid to move in a desired path without an extra pump and to induce complex flows for mixing. Few years later, the same group developed a better version of MHD micromixer with differential pumping capabilities for two different miscible fluids by applying different potentials to electrode pairs to create Lorentz-force with different sizes to drive the liquid to a desired direction for pumping and induce the liquid circulation at a cross-section for mixing [56].

2.6 3D printing approach and lithography-based approach for device fabrication

2.6.1 3D printing approach

After the expiration of an essential patent of 3D printing technology in 2009 [57], 3D printing has been rapidly developed and widely applied in various fields from the scientific research community to industry. It is a simple and accurate printing technology with reasonable cost and high printing efficiency that can easily make a computer-assisted design into a physical object with sizes ranging from micrometers to centimeters [58, 59]. Recently, the 3D printing technology has received attention in microfluidic devices [60], and it is a nickname of additive-based manufacturing techniques.

For microfluidic fabrication, the commonly used 3D printing techniques are selective laser sintering (SLS), fused deposition modeling (FDM, or named as “thermoplastic extrusion”), photopolymer inkjet printing, inkjet-based binder jetting, laminated object manufacturing (LOM), and stereo-lithography (SL). According to Au et al. [60], among these techniques, SL and LOM are more suitable for closed channel fabrication in microfluidics, and the others require the extra assembly process. The starting status of the material with SLS is powder. Fig. 2.6 illustrates the structure and working principle of SLS. The laser beam delivers energy to heat the powder. Instead of being melted, the powder will be fused by a laser beam [60]. By the way, SLS fabricated parts have various biomedical applications, e.g., scaffolds, drug delivery devices, models of prosthesis or organs for medical imaging data [60-62]. Compared with other 3D printing techniques, the sintered precursor powder leads to a higher purity and the properties of the printed part are close to those of traditional means. Different precursor materials can be combined to perform multi-materials printing. Besides, SLS can be adapted to write metal patterns onto polymers [63].

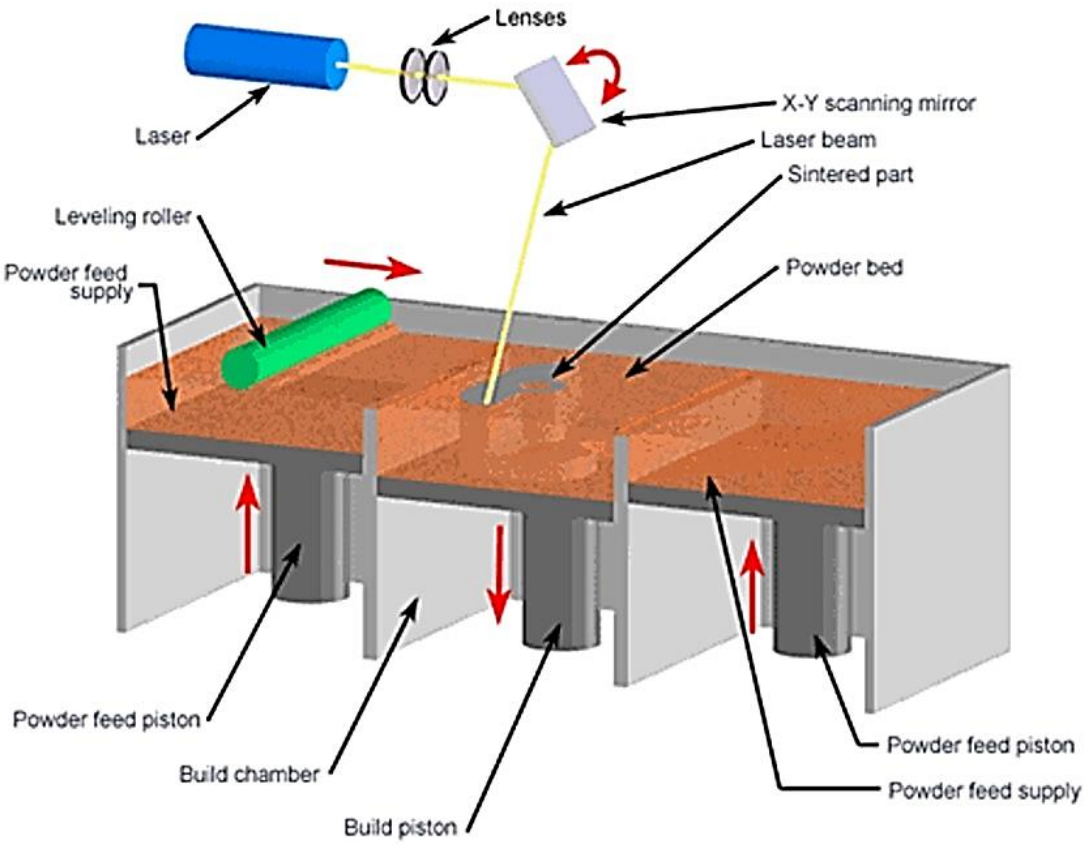

Fig. 2.6. Selective laser sintering [64].

Laminated object manufacturing (LOM) uses plastic, metal and ceramic laminates to fabricate devices by assembling the layers of the laser-cut materials with glues or chemical bonding. Fig. 2.7 illustrates the structure and working principles of LOM. During the bonding process, pins or special machines are applied to align and stack layers. Unlike other 3D printing techniques, LOM requires etching and assembling each layer [60] but the benefit with LOM is that it can readily work for metals and ceramic materials [65, 66].

Despite all the advantages, 3D printing also has limitations. For example, printing resolution is not as good as other fabrication techniques. Typically, the size range is around greater than 50 µm, and the accuracy can be around 50% error, see Table 2.3 [59]. Besides, some other problems for microfluidic fabrication via 3D printing cannot be

ignored considering the shape conformity of the printed structures, surface roughness, and the limitations of material [58].

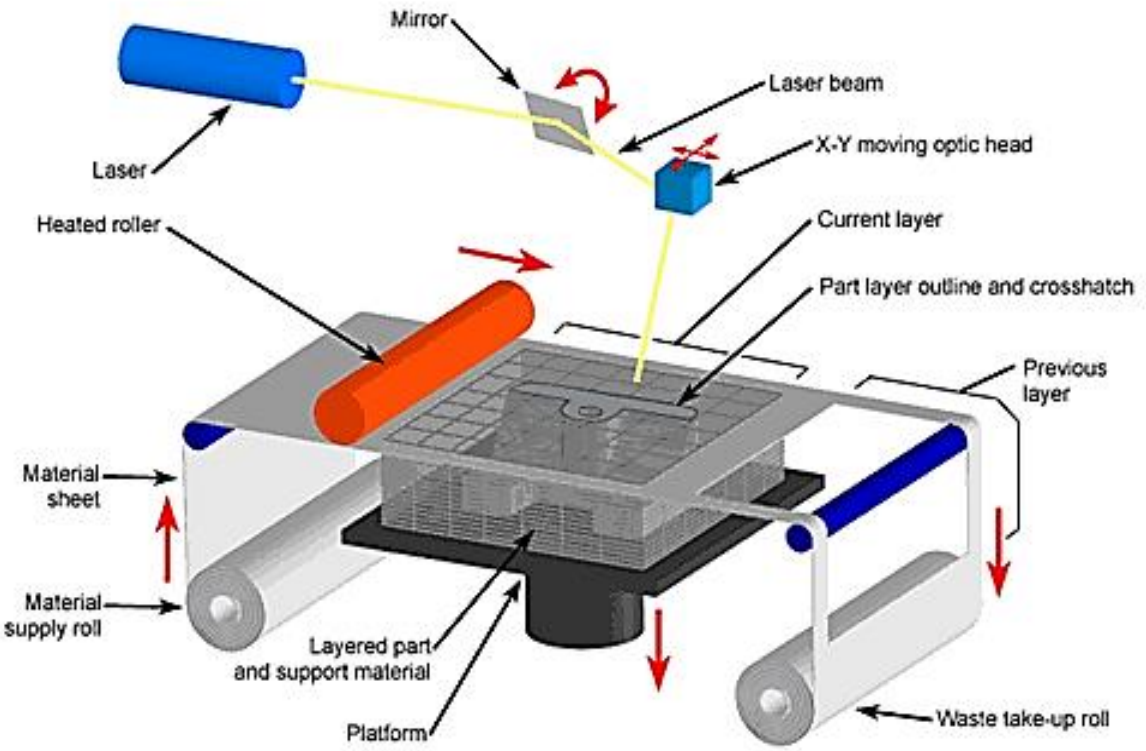

Fig. 2.7. Laminated object manufacturing (LOM) [67].

Table 2.3. Accuracy of 3D printed parts [59].

DESIGN	ACCURATE MODULE
Width < 100 μm Height < 50 μm	Collapsed structures
Width between 100-1000 μm Height between 50-500 μm	Width differences were around 35 μm, and height differences were less than 11 μm

2.6.2 Lithography-based approach

Lithography is employed to make 3D relief patterns on substrates. Inspired by the integrated circuit fabrication and semiconductor processing, the technology to fabricate the first MEMS started with substrates and layer processes. The structure with this technology is essentially planar. Fig. 2.8 illustrates the process for MEMS fabrication with photolithography and soft lithography approaches [68]. The materials of the wafer can be silicon, glass, quartz, metals and polymer films. A silicon substrate is employed, as shown in Fig. 2.8(A). Usually, a layer of silicon oxidation is thermally grown on the surface of the wafer. Then a thin layer of photosensitive material called photoresist is coated on the silicon oxidation through a process named spinning in Fig. 2.8(B). After that, a mask, or a photomask, which is characteristically made, is placed close to the wafer. Ultraviolet light is applied to shape the photoresist. Photoresists could be divided into two types: negative resist and positive resist. In negative resist, after exposure to UV lights, it hardens and is less soluble. The positive resist does the opposite. Unwanted parts of photoresists are removed by chemical solutions (also named as developers) and this process leaves windows to the oxidation layer. The remaining photoresist protects the selected regions of the oxidation layer, and the exposed region of oxidation layer is then etched and leaves a window to the wafer. Thus, regions on the wafer that is reacting with chemicals can be selected and controlled. Fig. 2.8(D) illustrates the master mold made through the conventional photolithography process [69].

With excellent biocompatibility, low cost, and good physio-chemical properties, PDMS is much suitable and commonly applied to the soft lithography process particularly in the area of microfluidic systems for components such as channels, valves and pumps [60]. When the master mold is fabricated in Fig. 2.8(E), a PDMS regent is cast onto the master mold. After it is thoroughly dried in the curing process, the PDMS layer is peeled off from the master mold, as shown in Fig. 2.8(F). In microfluidics, channels need to be bound, and to this connection, the PDMS layer needs to bind with another PDMS or glass. It is noted that bonding is usually enhanced by applying oxygen plasma treatment [70].

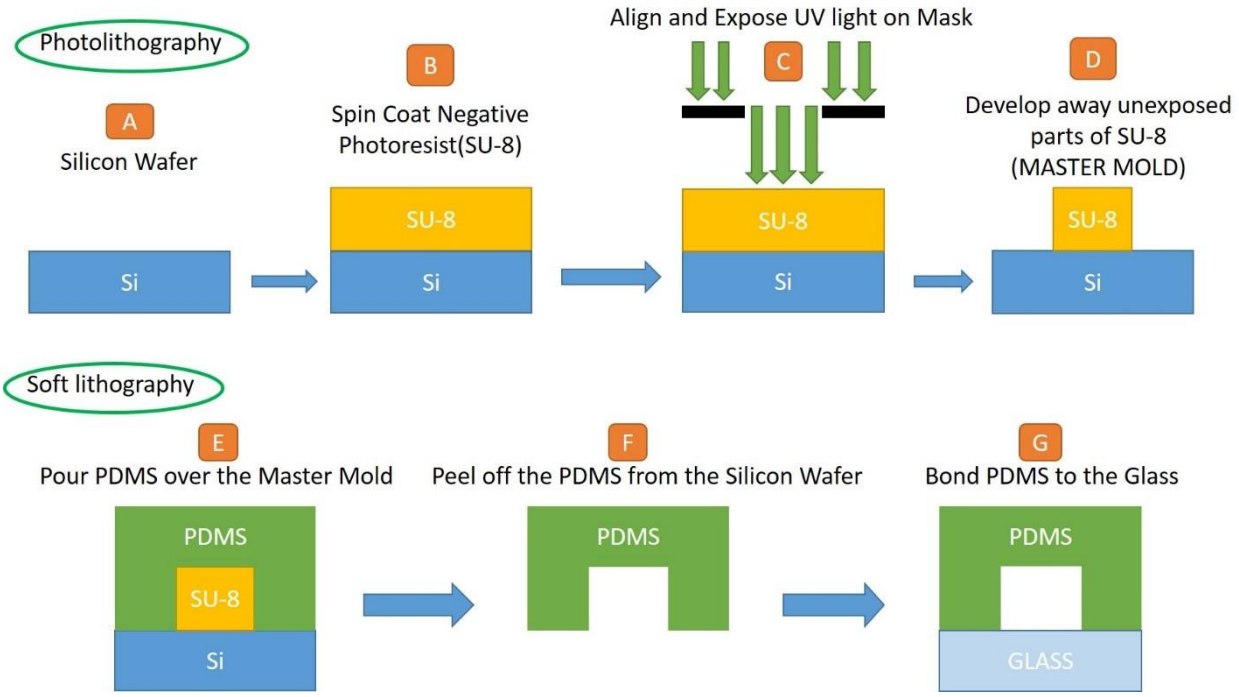

Fig. 2.8. The procedure of Photolithography and soft lithography [68].

2.7 General design methodology

A science-based design includes (i) General design phase theory, (ii) General design theory and methodology, and (iii) Design modeling and optimization. General design phase theory consists of technical specifications of the requirement, concept design, embodiment design, and detail design. Technical specifications of requirements refer to a document of customers' requirements in technical terminology. The specifications of design problems consist of a function specification and a constraint specification. Conceptual design focuses on developing the working principles of devices under design to satisfy customers' requirements in the technical specification. Embodiment design relates to activities to develop the body structure of the device to be designed to meet the requirements of the working principle [8]. Detail design involves a complete specification for each component to be ready to be manufactured [71, 72].

Requirements refer to functional requirements (FRs) and constraint requirements (CRs). FRs are the requirements of a function or functions that the device or system has to fulfill. CR is a condition or situation for a device or system to achieve FR [8]. In fact, CR is normally implicitly attached to FR. Design parameter (DP) is employed to describe the structural element to meet both the functional requirements and constraint requirements. For a large system or a complex device, the overall FR can be decomposed into FR1 and FR2 along with the DP decomposed into DP1 and DP2, where DP1 and DP2 fulfills FR1 and FR2, respectively in Fig. 2.9. The overall functional requirement can be fulfilled at different design phases. The relationship between FR and DP can be described by axiomatic design theory 1 (ADT 1), which will be mentioned in the following general design theory and methodology part [71-73].

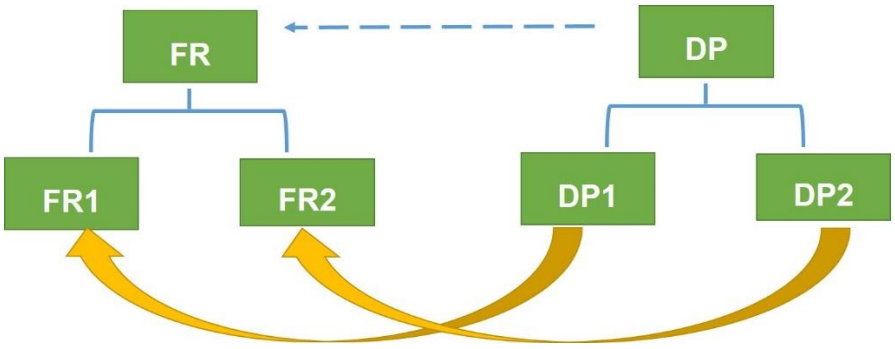

Fig. 2.9. Decomposition of FR and DP.

General design theory and methodology refer to axiomatic design theory, which has been verified by numerous applications. The first axiomatic design theory (independence axiom) is to guide what to do and how to do it separately, and to maintain the independence of functional requirements [71, 73].

Based on Axiom 1, the relationship between FRs and DPs is in the following [74, 75]:

$$FR=A\ DP \tag{2-1}$$

where A is called design matrix.

A further note is given to Equation (2-1). If the variation of FR and variation of DP with respect to their nominal values are very small, equation (1) can be further written by

$$d\,FR = A\,d\,DP \tag{2-2}$$

where d is the differential, FR is a vector of FR_i, and DP is a vector of DP_j, where i = 1, 2, …, n; j = 1, 2, …, m (n: the number of FRs; m: the number of DPs), and A is defined as

$$A_{ij} = \frac{\partial FR_i}{\partial DP_j} \tag{2-3}$$

where i = 1, 2, …, n; j = 1, 2, …, m.

Fig. 2.10 is the structure of the design matrix. According to Suh [74], designs can be uncoupled, decoupled and coupled. If the design matrix was diagonal, this design is an uncoupled. That is the FRs can be satisfied by DPs independently; besides, the FRs remain independent. If the matrix was triangular, the design is decoupled. In decoupled design, the FRs can only remain independent when the DPs are operated properly. If the design matrix was in any other forms differing from diagonal or triangular, the design is defined as a coupled design.

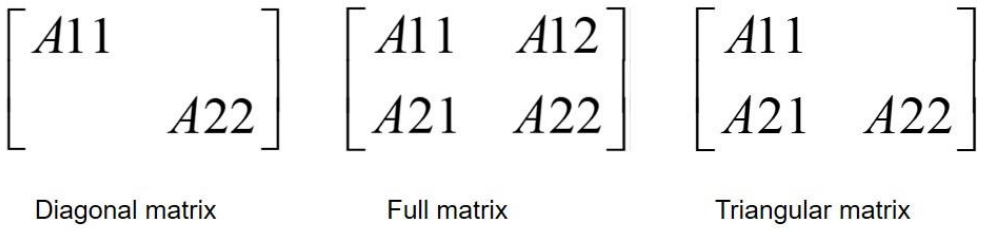

Fig. 2.10. The structure of the design matrix.

Based on Axiom 1, the better design should meet [74, 76]: (1) Design or function requirements (FRs) should be independent or uncoupled on their own right; (2) Design parameters (DPs) should maintain the independence of FRs – i.e., not making FR coupled. Thus, to satisfy the independence axiom, the design matrix must be either diagonal or triangular.

Axiom 1 involves concept design, which is also called logical design. Design modeling and optimization refers to [74, 76]: (1) Mathematical model for design objects at a different level (conceptual object, embodiment object, detailed object); (2) Variables defined for

structural features, and mathematical relations defined for the whole structure along with its behavior; (3) Varying of the variables to seek the best behavior.

2.8 Conclusions

Based on the above discussion, it can be concluded that the existing microfluidic devices can only perform one or more functions, e.g., pumping function, particle mixing function, and particle separating function, with each function being performed in a distinct time stamp. In particular, there are still unnecessary transportations of samples from one functional unit to another functional unit. Therefore, the development of microfluidic devices by eliminating transportations is needed, which is called integrated functional device.

Chapter 3: Design

3.1 Introduction

This chapter presents the systematic design process for the novel multi-functional device, including the functions of pumping, particle separating, and particle mixing. The design process consists of requirement analysis in Section 3.2, conceptual design in Section 3.3, embodiment design and detail design in Section 3.4. The conclusion is presented in Section 3.5.

3.2 Design requirement

This novel multifunctional microfluidic device is required to perform pumping, particle separating, and particle mixing functions, and perform two or three functions simultaneously or without unnecessary transportations. This is called overall function requirement in the literature of design theory and methodology [71]. This overall FR was decomposed into

- FR 1: to provide the driving pressure for samples to flow within the device.
- FR 2: to mix two different sizes of particles[1].
- FR 3: to separate two different sizes of particles.

FR 2 is further decomposed into

- FR 2.1: to provide active stirring.
- FR 2.2: to make a long mixing path.
- FR 2.3: to make samples have long residence time within the channel.

FR 3 is further decomposed into

- FR 3.1: to provide driving pressure for particles to flow to the outlet of the device.
- FR 3.2: to let only one type of particles stay in the main channel.

[1] In this thesis, cells and particles are used interchangeably.

The constraint requirements (CRs) are:

- CR 1: The size of elements of the microfluidic device is in microscale.
- CR 2: Particles under separation have different sizes and deformability.

3.3 Conceptual design

Design parameters (DPs) of the device are descriptions of structural elements of the device to meet both the functional requirements (FRs) and constraint requirements (CRs) [71]. DPs were proposed to fulfill the FRs and CRs, and they are presented in the following.

For FR1, there are two design options: DP1a: a main channel with deformable membranes A and B connecting to it. Membranes A and B deflect alternately by injecting and aspirating water into and out of the chambers, which connect to the membranes A and B, thus providing the driving pressure for fluid to flow within the main channel. DP1b: two membranes attached with a cylinder-shaped bulk magnate and EM coils (Figure 2.2 in Chapter 2); when the current of the EM coil is on and off alternatively, the membrane attached with the magnate deflects to provide the driving pressure alternately. In this research, DP1a was chosen because it can facilitate the fabrication, minimize the overall size of the device, and meet the constraint requirement CR1.

To fulfill FR 2, there are two design options: DP2a: a main channel alongside with a circulating channel, in which two types of particles mix together; the deformable membranes A and B provide the driving pressure for the samples to flow within the circulating channel and main channel. DP2b: a long mixing path with membrane D, E, and F, on which a magnate is attached and the EM coil (see Figure 2.2 in Chapter 2). In this research, DP2a was chosen because it meets the constraint requirement CR1.

For FR 3, there two design options: DP3a: a main channel alongside a circulating channel, in which two types of particles mix with each other, is extended to the channel with the deformable membrane C, which deflects to allow particles with a certain size to pass

through the channel. DP3b: one main channel for the sample solution, two focusing channels, two detecting channels, one pumping channel and one collecting well, and a resistance pulse sensing gate (see Figure 2.4 in Chapter 2). The two detecting channels are used to control particles moving at the center of the main channel so that the particles can pass through the sensing gate one at a time, and detect resistance changes when particles pass through the sensing gate. The pumping channel is used to pump the target particles into the collecting well. In this research, DP3a was chosen because it meets both the constraint requirement CR1 and the constraint requirement CR2.

In summary, the conceptual design of the multi-functional device with pumping, particle separating, and particle mixing functions is the aggregation of DP1a, DP2a, and DP3a.

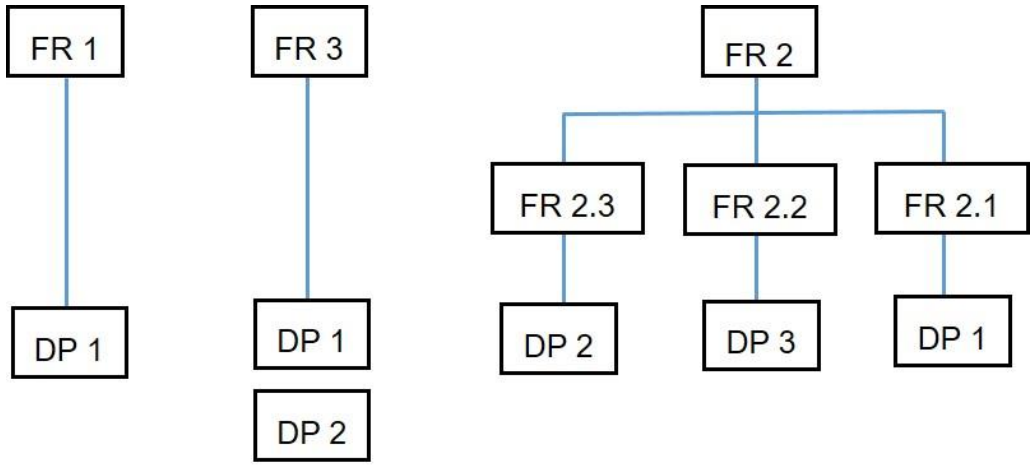

Fig. 3.1. The relationship between FRs and DPs.

From Fig. 3.1, the relationship between FRs and DPs can be shown in the following matrix:

$$\begin{bmatrix} FR\ 1 \\ FR\ 2 \\ FR\ 3 \end{bmatrix} = \begin{bmatrix} A11 & 0 & 0 \\ A21 & A22 & A23 \\ A31 & A32 & 0 \end{bmatrix} \times \begin{bmatrix} DP\ 1 \\ DP\ 2 \\ DP\ 3 \end{bmatrix} \quad (3\text{-}1)$$

From Equation (3-1):

- FR1=A11×DP1,
- FR2=A21×DP1 + A22×DP2 + A23×DP3
- FR3=A31×DP1 +A32×DP2

From the above equations, one can obtain:

- Step 1: Any changes to DP1 will affect FR1, FR2, and FR3.
- Step 2: Any change to DP2 will affect FR2 and FR3.
- Step 3: Any change to DP3 will affect FR2.

Step 1 also affects FR3. But in Step 3, this effect is changed back and FR3 is further affected by DP2 only.

From the above analysis, it can be concluded that the design is a decoupled design. According to Axiom 1 of Axiomatic Design Theory (ADT) [71-75], this is an acceptable or good design.

To develop the body structure of the device to meet the requirements of the working principle, the deformable membrane is designed as shown in Fig. 3.2. Each membrane connects with a chamber in which water or gas will be injected to cause pressure changes and provide pressures for the membranes to deflect. The deformable membranes will provide the driving pressures for the sample within the channel to move as well as form a gate to allow the designed size of particles to pass.

DPs are integrated to build the body structure of the whole device, as presented in Fig. 3.3. The device consists of one main channel, one circulating channel, three deformable membranes, an inlet, and an outlet in Fig. 3.3.

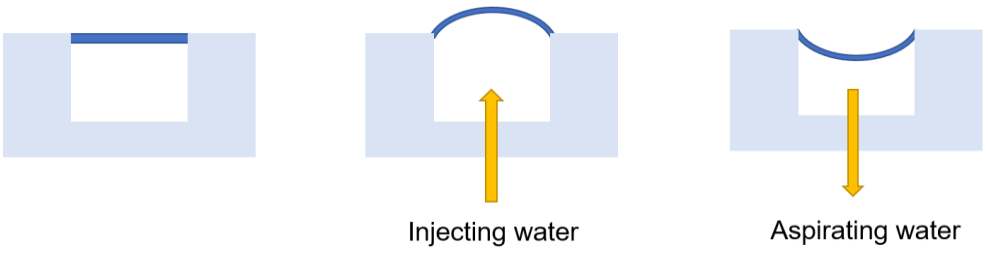

Fig. 3.2. Deflection of the membrane. (a) Initial position of the membrane. (b) Membrane deflects when injecting water into the chamber. (c) Membrane deflects when aspirating water out of the chamber.

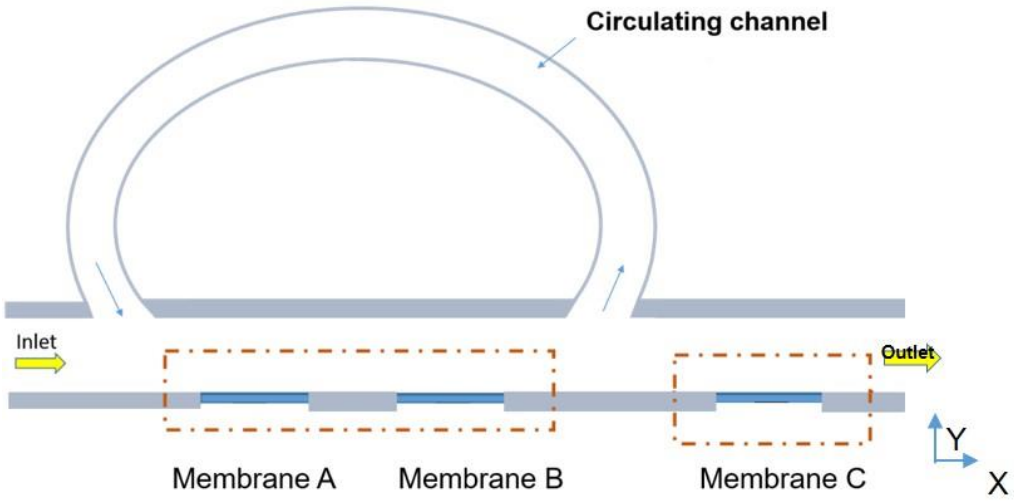

Fig. 3.3. The integration of DPs. Z-direction is the gravity direction.

The pumping, mixing and particle separating functions can be fulfilled by the proposed device in Fig. 3.3. The pumping function can be achieved via injecting water or gas into the chamber and aspirating water or gas out of the chamber. The alternation of the injecting and aspirating behaviors helps the membranes to deflect and to provide the driving pressure for the sample to flow within the device.

As for particle separation, particles can be sorted based on the size difference and particle deformability difference between the target particles and the others, simply in the condition of $D > \Delta d$, where D is the diameter of the target particles, and Δd is the distance between the deflected membrane C and the main channel, as shown in Fig. 3.4.

The particle separating function requires several steps. Step 1: Membrane C deflects in a condition where Diameter of target particle > Δd as Fig. 3.4 presents by injecting water into the chamber of membrane C. Step 2: injecting the sample which contains two different sizes of particles (the target particle A and the other particle B, where the diameter of particle A is larger than that of particle B). Step 3: injecting water into the chambers of membrane A and B, and aspirating the water out of the chambers of membrane A and B alternately and continually.

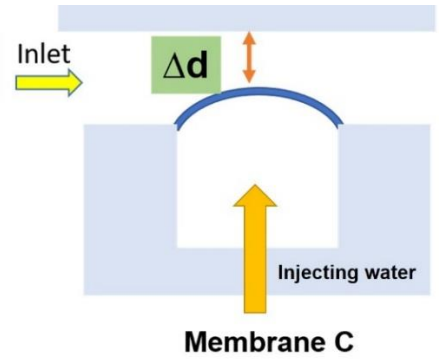

Fig. 3.4. The deflection of membrane C.

For example, due to the size difference and cell deformability difference between the circulating tumor cells (CTCs) and normal blood cells, the procedures to separate CTCs from the blood sample of patients with colorectal cancer are as follows [77]. First, water will be injected into the chamber of the membrane A,B and C, respectively, so that the membrane C will deflect as shown in Fig. 3.4 in the condition of $D_{(CTCs)} > \Delta d \geq D_{(normal\ blood\ cell)}$ where $D_{(CTCs)}$ is the diameter of the circulating tumor cells, Δd is the distance between menbrane C and main channel, and $D_{(normal\ blood\ cell)}$ is the diameter of normal blood cells. The membrane A and B in Fig. 3.3 will deflect to provide the driving pressure for the sample to flow within the channels. Then the sample, which contains CTCs and other blood cells, will be injected into the main channel. Some normal blood cells will flow to the outlet; meanwhile, due to the size difference and cell defomability difference, CTCs will remain in the main channel and flow into the circulating channel along with some normal blood cells. Then, the CTCs and the normal blood cells will flow through the main channel and circulating channel again to repeat a circulation. After several circulations, the remaining particles in the main channel and the circulating channel will be CTCs.

When comes to mixing function, as the device is designed to mimic cellular activities, the mixing behavior focuses on mixing particles with particles, for instance, mixing circulating tumor cells with anti-cancer drugs. The drug can be injected to the main channel to mix with CTCs which are selected and remain in the main channel and circulating channel, while the membrane C remains to be deflected in the condition of $D_{(CTCs)} > \Delta d$ where $D_{(CTCs)}$ is the diameter of the circulating tumor cells, Δd is the distance between menbrane

C and main channel of Fig. 3.4. The other two membranes A and B will go up and down alternatively to perform pumping and particle mixing functions. Meanwhile, the target cells will remain in the mixing chamber for full mixing. A better mixing requires active stirring, mixing path and residence time for mixing, and all these requirements can be achieved by the deformable membranes, the main and circulating channels, and deformable membrane C to close the main channel.

3.4 Embodiment design and detail design

Fig. 3.5 is the schematic of the design in X-Y plane. The multi-layer structure of the device design could lead to leakages of the device. The more layers of the device, the more probability of leakages [78]. So, the device was proposed to have two layers. The first layer, also called substrate, is a piece of glass. The second layer is the main body of the device, and the material of it is Polydimethylsiloxane (PDMS). All the components of the device were proposed to lay out in the X-Y plane, and thus the device was horizontally laid out to decrease the chances of leakage caused by the alignment and bonding of layers. The more layers of the device will lead to a greater chance of leakage. As shown in Fig. 3.5, in the X-Y plane, in agreement with the size and deformability of CTCs mentioned in Section 2.4, the main channel was proposed to be 30 μm in width, and the circulating channel was gradually increased, in a trial-and-error manner, from 30 μm in width to 80 μm in width. The membranes A and B functioning as pumping and particle mixing membranes, which are connected to the main channel are 200 μm in length and 10 μm in thickness. The membrane C performing particle sorting and mixing is 300 μm in length and 10 μm in thickness. The chambers of the membranes A and B is 200 μm in both length and width. The chamber of membrane C is 200 μm in width and 300 μm in length. The channels of the chambers which connecting to membrane A and B are 150 μm in width. The channel connecting to membrane C is 200 μm in width. The total height of the channel in Z direction is 50 μm. The device is bonded on a glass substrate.

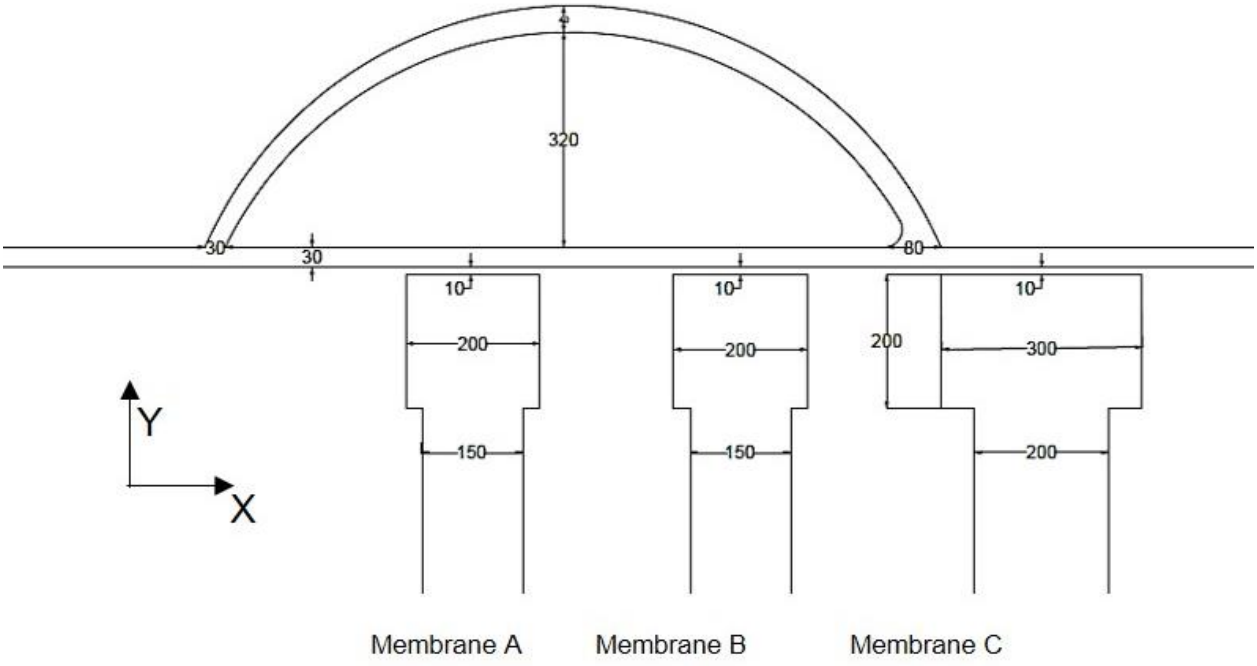

Fig. 3.5. The schematic of the device in X-Y plane (dimension in μm).

3.5 Conclusions

This chapter shows the design process and the details of the integrated multi-functional device. The pumping, particle sorting, and particle mixing functions can be fulfilled by injecting and aspirating water into and out of the chamber of the deformable membranes A and B. Thus, the membrane deflects to provide pressure difference within the main channel as well as to act as a gate or a switch to partially close the main channel to let only the designed size of particle remain in the main channel and the rest of the particles can pass through the gate. The mixing process can be enhanced by increasing the residence time of the particles within the device, and active stirrer. Based on the discussion above, it is practicable that the designed device can fulfill the pumping, particle sorting, and particle mixing functions.

Chapter 4: Modeling and Simulation

4.1 Introduction

The modeling and simulations of the deformable membranes of the device are presented in this chapter. The design was discussed in Chapter 3, and it can be known that the membrane is the key element; therefore, the modeling and simulation were restricted to test the deformability of the membrane with different thicknesses, lengths, and pressure loads on the membranes. The loads were generated via injecting water or gas into the chambers, which connected to the membranes. The software COMSOL Multi-physics 5.3a software (COMSOL Inc., Burlington, MA, USA) was applied to build the model and simulate the behaviors and performances of the membranes with different membrane lengths, thicknesses, and boundary loads. Section 4.2 focuses on the schematic model of the membrane. Section 4.3 shows the governing equations for the membrane deflection. Section 4.4 presents the modeling of the membrane in COMSOL. Section 4.5 presents the simulation results. Section 4.6 presents the conclusion of this chapter.

4.2 The schematic model of the membrane

As mentioned above, the simulation was performed on the deformable PDMS membrane. The schematic model of the membrane for simulation is presented in Fig. 4.1. Fig. 4.1(a) is the original 3D model of the integrated device. As shown in Fig. 4.1(b), the various pressure loads were acted on the membranes. One fluid is in the main channel and the other one is in the chambers. The final schematic model considered for simulation was given in Fig. 4.1(c), where the boundary pressure, which is provided through injecting water or gas into the chambers, is considered to be the boundary load.

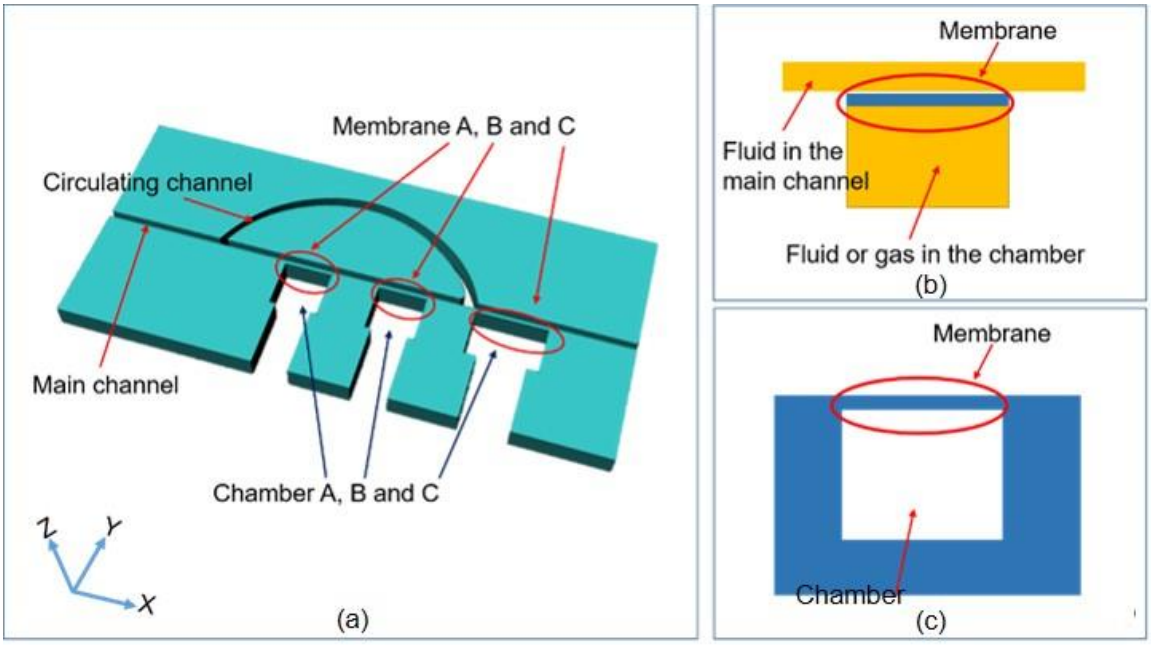

Fig. 4.1. (a): The schematic model of the multi-functional device: the height of the device is in Z direction, the width of the device as well as the thickness of the membranes is in Y direction, and the length of the channel and the device is in X direction. (b): Interaction between the membrane and fluids. (c): The membrane chamber.

4.3 Governing equations

The PDMS membrane to be simulated was considered as a solid system in this study. The PDMS membrane is considered as a hyper-elastic material (e.g., rubber) and the governing equation is given [79]:

$$\rho \frac{\partial^2 u_{solid}}{\partial t^2} = \nabla \cdot (FS)^T + FV, F = I + \nabla u_{solid} \quad (4.1)$$

$$S = S_{ext} + \frac{\partial W_s}{\partial \epsilon}, \sigma = j^{-1} F S F^T, j = det(F) \quad (4.2)$$

$$\in = \frac{1}{2}(F^T F - I) \quad (4.3)$$

$$W_S = C_{10}(I_1 - 3) + C_{01}(I_2 - 3) + \frac{1}{2}\kappa(j_{el} - 1)^2 \quad (4.4)$$

where S is the second Piola-Kirchhoff stress tensor, and V is the volume, W is the strain energy density function, F is the force applied to the material, ε is the strain ratio, and C is the material constant. In this simulation, the value of C_{10} and C_{01} were taken as 0.07 MPa and 0.008 MPa, respectively, according to Yu *et al.* [79].

4.4 Model Development with COMSOL

There are several steps to build a finite element model of the membrane. First, building a 3D geometry of the target membrane. Second, defining the material of the membrane. Third, defining the boundary condition and boundary load. Then building mesh.

In Fig. 4.1(c), the system was a solid system. Fig. 4.2 is the 3D geometrical shape of the membrane. The different membrane lengths, thicknesses and boundary loads on the membrane were examined. Four different lengths: 50, 100, 200, and 300 μm, and four different membrane thickness: 5, 10, 30, and 50 μm. Besides, the boundary pressure is from 1500 mbar to 8000 mbar. The height of the membrane, also known as the height of the channel is 50 μm.

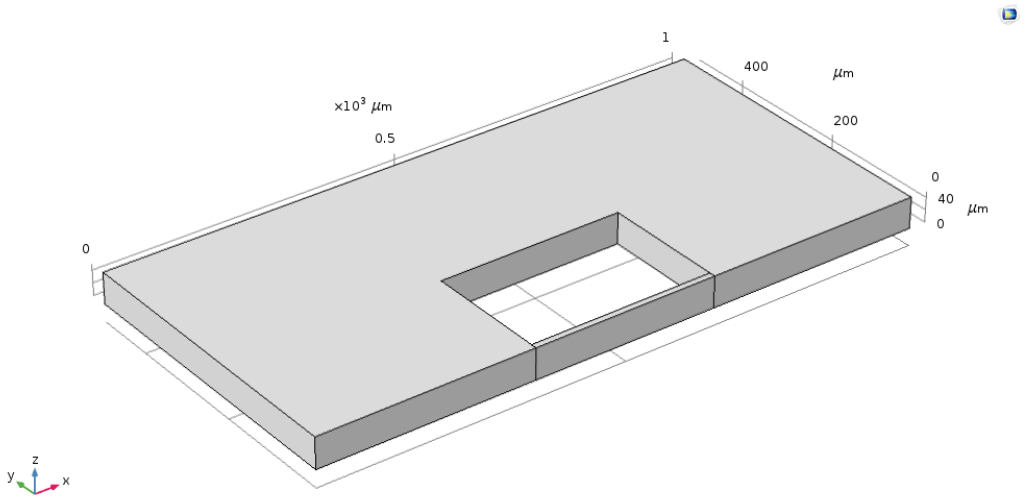

Fig. 4.2. The geometrical shape for the membrane with a thickness of 10 μm, length of 300 μm and membrane load of 5800 mbar. Channel height of 50 μm. Membrane

thickness: along Y-axis; membrane length: along X-axis; Device height: along Z-axis.

The material defined for the system in COMSOL was PDMS. The fixed constraint of the system is showed in Fig. 4.3(a), and the attachment of the membrane layer is shown in Fig. 4.3(b). Besides, the attachment of the membrane to the main body was the rigid connection. The pressure was loaded on one side of the membrane as shown in Fig. 4.4.

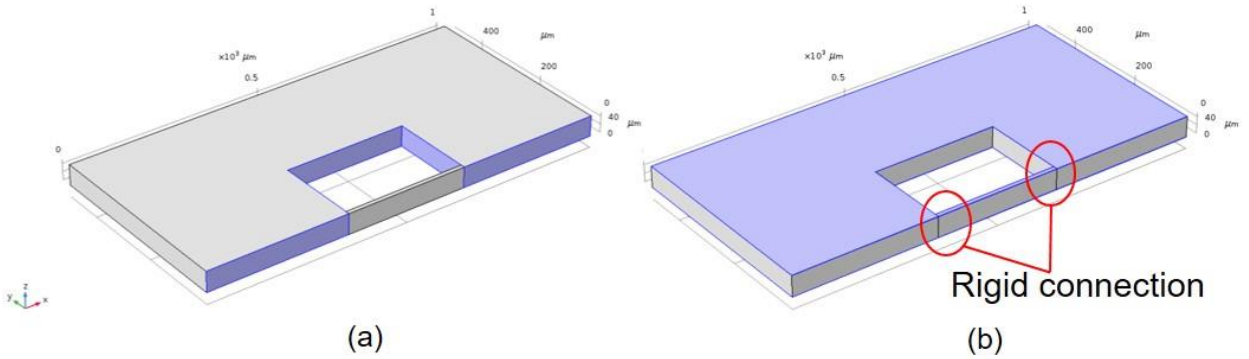

Fig. 4.3. The fixed constraint and attachment of the system. Membrane thickness: along Y-axis; membrane length: along X-axis; Device height: along Z-axis.

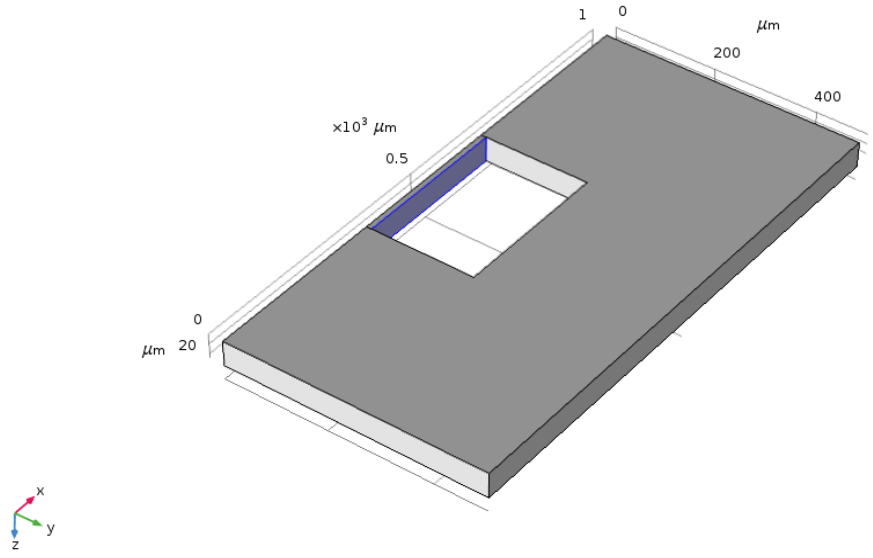

Fig. 4.4. The boundary load on the membrane. Membrane thickness: along Y-axis; membrane length: along X-axis; Device height: along Z-axis.

The mesh of the system is a user-controlled mesh in Fig. 4.5. The domain of the membrane and the domain of the rest of the chamber were covered by different meshes. A nonuniform mesh of quadrilateral elements was used to discretize the membrane with the extra fine grids and the rest of the chamber with normal grids. The mesh was getting coarser further away from the membrane. After building the model of the target system in COMSOL, the different thicknesses and lengths, as well as boundary loads, were examined in simulation. With a study of “stationary” study in COMSOL, the deflections of the membranes were presented in the “results” of the COMSOL. Besides, for the pressures from 1500-8000 mbar, which were examined in this study, “parametric sweep” was adopted in COMSOL.

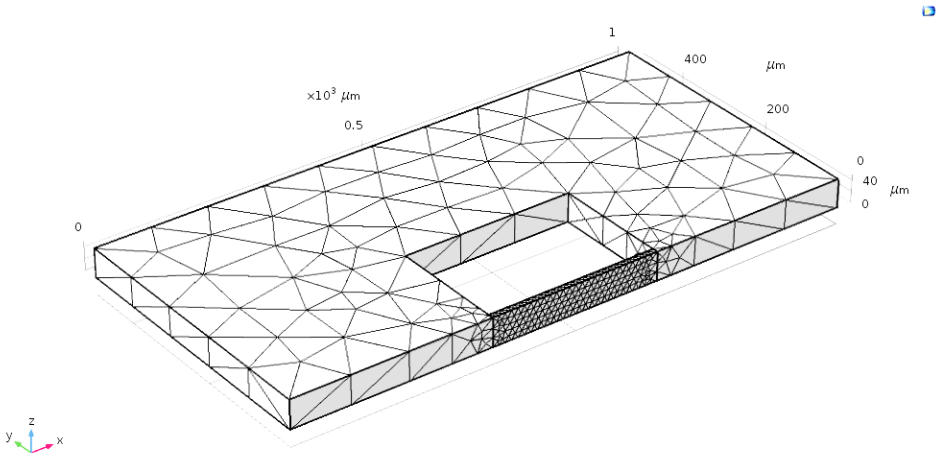

Fig. 4.5. The mesh of the simulated system. Membrane thickness: along Y-axis; membrane length: along X-axis; Device height: along Z-axis.

4.5 Results with Discussions

The simulation results of the target system helped to predict the performance of the membranes with different thicknesses, lengths and boundary loads. The simulation model was verified by comparing the simulation results with the experiment results, which are presented in Table 4.1. It is worth mentioning that the experiment will be presented in Chapter 5. The simulation model was developed, and the results from the simulation using the finite element analysis agreed well with the experiment data. Fig. 4.6 presents

the experiment results and simulation results with the membrane thickness of 10 μm, the length of 300 μm, the membrane height of 50 μm, and the membrane boundary load of 5828.71 mbar. The deflection experiments were conducted by injecting gas into the membrane chamber via a micropump (FOUR-CHANNEL PRESSURE VACUUM CONTROLLER OB1 MK3+, World of Lab Technologies Co., Ltd, China). The visualization was completed via an inverted biological microscope (SW-2000, Beijing PDV Instrument Co., LTD, China).

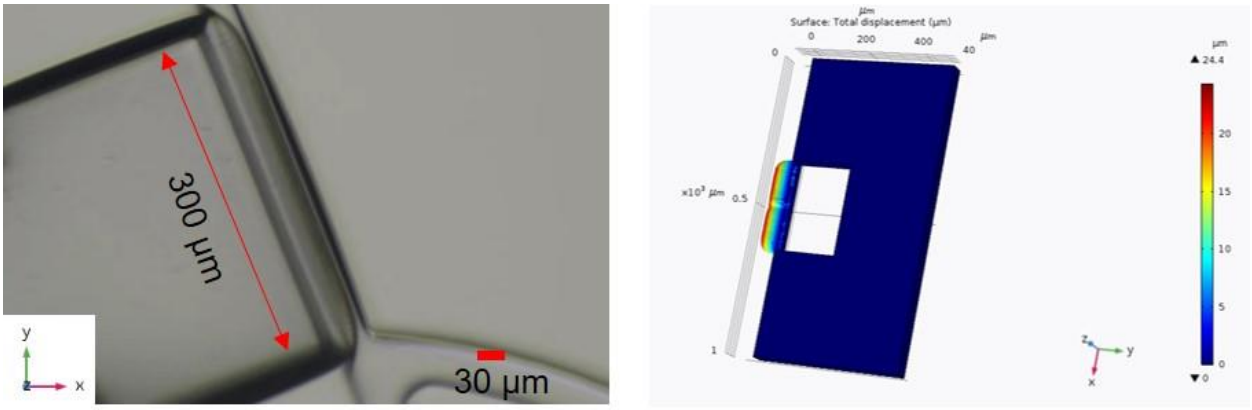

(a) (b)

Fig. 4.6. The experiment results (a) and simulation results (b) with membrane thickness of 10 μm, length of 300 μm, membrane height of 50 μm, and membrane boundary load of 5828.71 mbar.

Table 4.1. The comparison between the simulation result and the experiment results with the membrane thickness of 10 μm, membrane length of 300 μm, and membrane height of 50 μm.

Membrane length (μm)	Membrane thickness (μm)	Boundary load (mbar)	Deflection (μm)	
			Simulation	Experiment
300	10	5282.71	24.4	23.5±2.7

The deflection of the membrane with a thickness of 10 μm, a length of 300 μm, the boundary load of 5828.71 mbar and membrane height of 50 μm were 24.4 μm from the simulation model and 23.5±2.7 μm from the experiment results. The simulation results were in accordance with the experiment results, which shows that the simulation is accurate.

Figure 4.7 shows the simulation results of the deformable membrane with the thickness of 10 μm, the boundary load of 5500 mbar, and the lengths of 50, 100, 200, and 300 μm. The maximum deflection of the membrane is 24.5 μm with the membrane thickness of 10 μm, the length of 300 μm, and the boundary pressure of 5500 mbar.

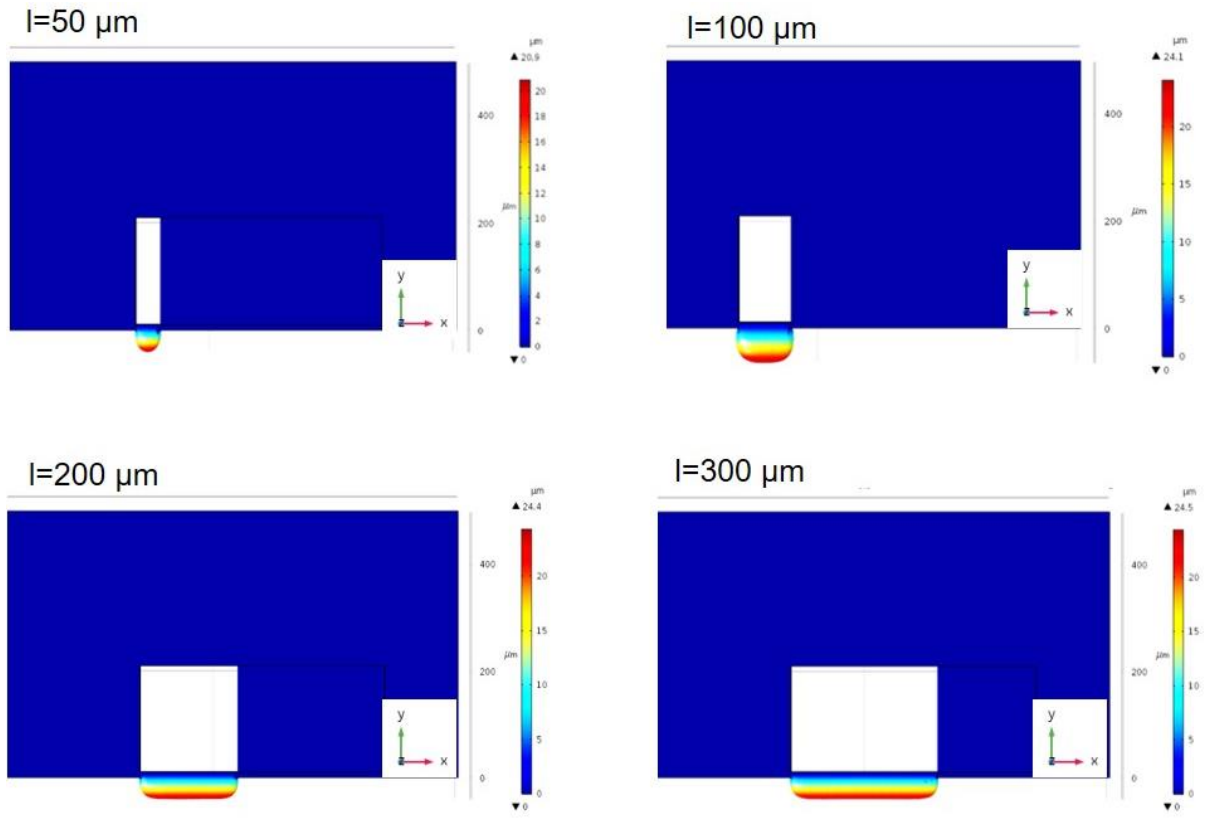

Fig. 4.7. Deflection of the membrane with the thickness of 10 μm, the boundary load of 5500 mbar, and the length of 50, 100, 200, and 300 μm:

Figure 4.8 presents the simulation results of the deformable membrane with the membrane pressure load of 1500 mbar, the membrane length of 300 μm, and the

membrane thicknesses of 5, 10, 30, and 50 μm. The maximum deflection of the membrane is 21.5 μm with the thickness of 5 μm, the length of 300 μm, and the boundary pressure load of 1500 mbar.

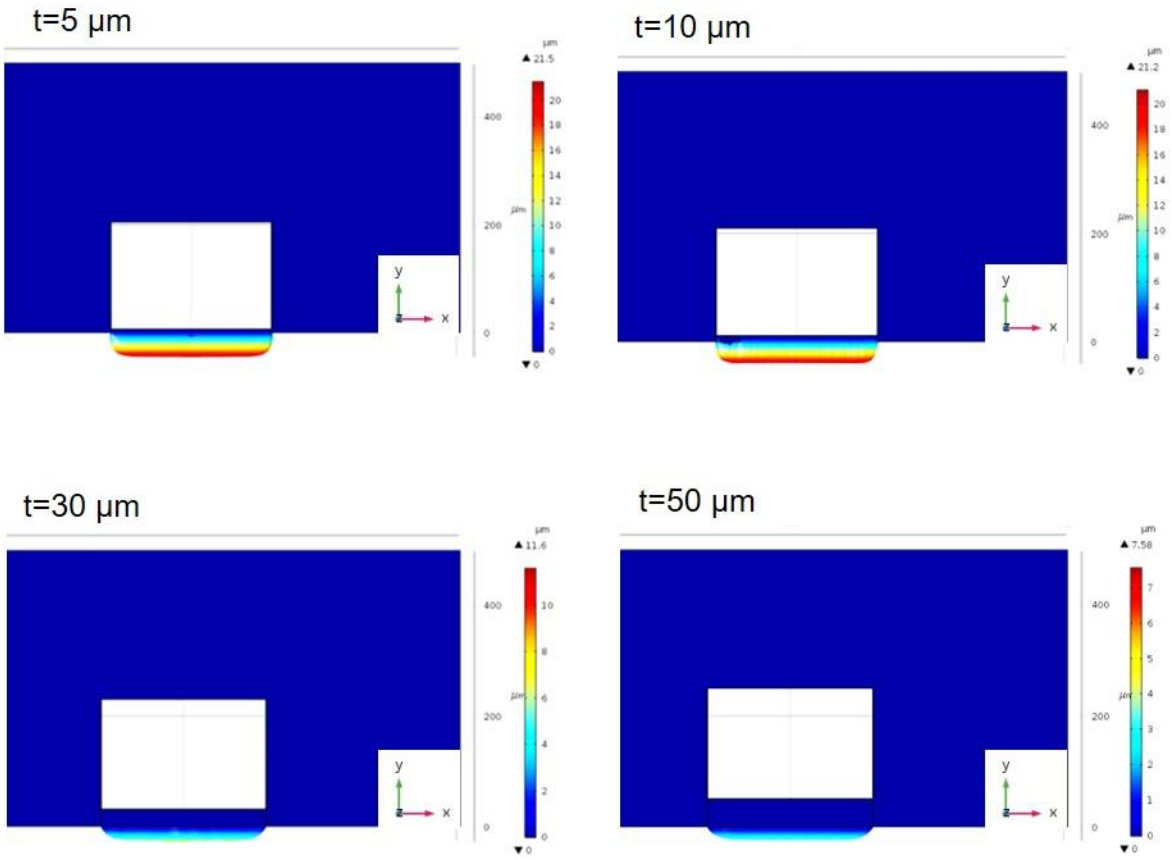

Fig. 4.8. Deflection of the membrane with the pressure load of 1500 mbar, the length of 300 μm, and the thicknesses of 5, 10, 30, and 50 μm.

Figure 4.9 shows the simulation results of the membrane deflection with the membrane length of 300 μm, the membrane thickness of 10 μm, and the pressure load of 1500, 3000, 5000, and 8000 mbar. The maximum deflection of the membrane is 25.7 μm with the thickness of 10 μm, the length of 300 μm, and the boundary pressure load of 8000 mbar.

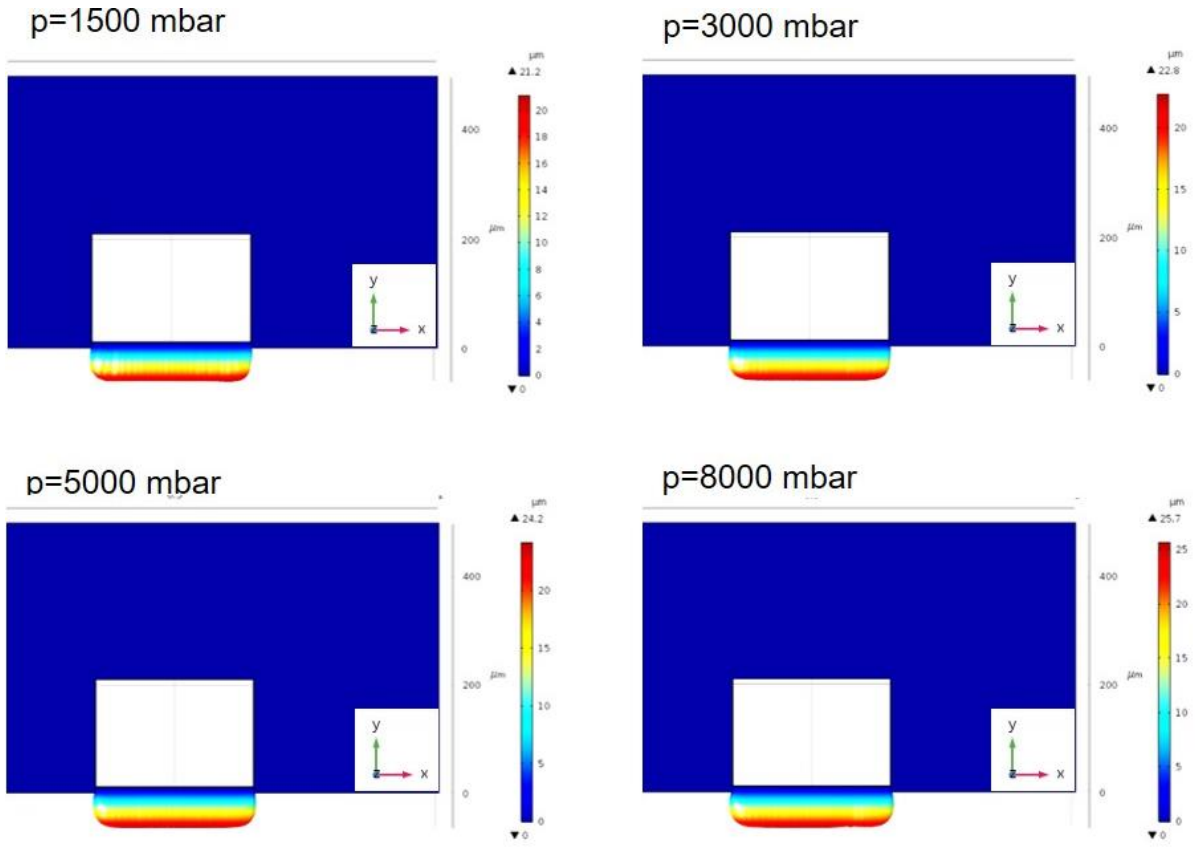

Fig. 4.9. Deflection of the membrane with the length of 300 μm, and the thickness of 10 μm, and the pressure load of 1500, 3000, 5000, and 8000 mbar.

4.6 Conclusions

The simulations of the membrane deflection with different membrane lengths, thicknesses and boundary loads were presented in this chapter. According to the simulation results, the deflection requirements of the membrane, i.e., to partially close the main channel, can be achieved. To validate the simulation model, the preliminary experiments were conducted, and the simulation result was found in agreement with the experiment result. The deflection of the membrane changes with the change of the thicknesses of the membrane, and the boundary loads on the membrane; specifically, an increase of the membrane length leads to an increase of the membrane deflection; besides, an increase of the boundary load on the membrane causes an increase of membrane deflection. Another validation of the simulation model is that the membrane thickness affects the

membrane deflections; specifically, if the thickness of the membrane increased, the deflection of the membrane decreases significantly.

Chapter 5: Fabrication and Assembly

5.1 Introduction

This chapter will discuss the fabrication and assembly of the prototype of the device. The fabrication and assembly were completed via UV light lithography and soft lithography at the Biomedical Science and Technology Research Center (BSTRC) and the Biomedical Science and Technology Center, both located at Shanghai University in Shanghai, and the research center of the company ZHONGXINQIHENG (cchip) in Suzhou. Both centers are the collaborator of the group at the University of Saskatchewan. Section 5.2 presents a comparison between the 3D printing approach and the lithography-based approach for the fabrication of the microfluidic device. Section 5.3 describes the fabrication process of the device. Section 5.4 describes the assembly of the device. Section 5.5 concludes this chapter.

5.2 A comparison of the lithography-based approach and the 3D printing approach

As discussed in Chapter 2, compared with the lithography-based approach, the 3D printing approach is simpler and more efficient to fabricate microfluidic device. The lithography-based approach requires manual operation and the processes for fabrication are more complex, while the 3D printing approach can easily fabricate a computer-assisted design into a physical object [58, 59]. Besides, the printing resolution of 3D printers can be micrometers, and even nanometers. The techniques of the lithography-based approach have been well developed and are mature to fabricate microfluidic devices with various design requirements, while 3D printing approach, which is applied for microfluidic device fabrication in recent years, has some problems in printing resolution compared with lithography-based technique. The printing accuracy can have around 50% error when the printing size range is greater than 50 μm [59]. Besides, compared with the lithography-based approach, the shape conformity of the printed structures, surface roughness, and limitations of the material of 3D printing approach cannot be ignored.

Based on the design requirements of the multi-functional microfluidic device, the membrane of the multi-functional microfluidic device requires to be fabricated accurately, which plays a key role in the function performing.

5.3 Fabrication

The fabrication approach for the multifunctional microfluidic device is a combination of photo-lithography and mold techniques, reviewed in Chapter 2, because the resolution of the 3D printer, TWO-photo polymerization (Nanoscribe GmbH, Kadsruhe, Germany) in this case, is too small to print the device in microscale. The following are details of the fabrication process.

Step 1: to clean the silicon wafer

A four-inch silicon wafer was soaked for 15 minutes in the mixture reagent (concentrated sulfuric acid and hydrogen peroxide with a mixing volume ratio of 3:1). Then the silicon wafer was cleaned by applying ultrapure water, absolute alcohol, and acetone respectively and was put on a heating machine (MB Digital Thermostat Heating Panel, ZHONGXINQIHENG-cchip, China) with the heating temperature of 200℃ for 5 minutes.

Step 2: to coat the negative photo-resistance on the silicon wafer

A negative photo-resist material SU-8.2050 was used to coat on the surface of the silicon wafer via a coating machine (KW-4A Spin Coater, ZHONGXINQIHENG-cchip, China), of which the speed and time were set as 2500 rpm and 30 s, respectively. Fig. 5.1 shows the result of the coating process.

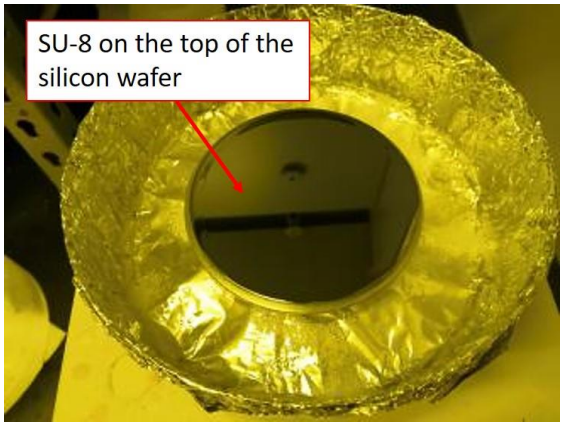

Fig. 5.1. The silicon wafer coated with SU-8.2050.

Then, the silicon wafer with SU-8.2050 was placed on a drying Plate (Hot Plate BP-2B, ZHONGXINQIHENG-cchip, China) with a heating temperature of 65℃ for 3 minutes as shown in Fig. 5.2. Before proceeding to the next step, the wafer needs to be cooled down to room temperature.

Fig. 5.2. Heat the silicon wafer coated with SU-8.2050.

Step 3: UV light exposure

The wafer, after the coating process, was placed under the UV light for exposure covered by a film photomask. The photomask was bought from a photomask fabrication company (Kunshan Kaisheng Electronics, China). The UV light machine was the Mask Aligner (URE-2000/35, ZHONGXINQIHENG-cchip, China). The dose was 20 mj/cm^2 and the exposing time was 6 minutes. After that, the whole system was baked for 3 minutes with

the backing temperature of 65℃. The whole system was cooled down to room temperature and was prepared for development.

Step 4: development

The UV light exposed photo-resistive system was then put in a bath filled with Su-8 developer in Fig. 5.3. The bathing process was repeated 3 times. After the whole system was put for baking with the baking temperature of 95℃ and baking time for 5 minutes. Fig. 5.4 shows the product of the device by now, and it was the master mold for the device designed.

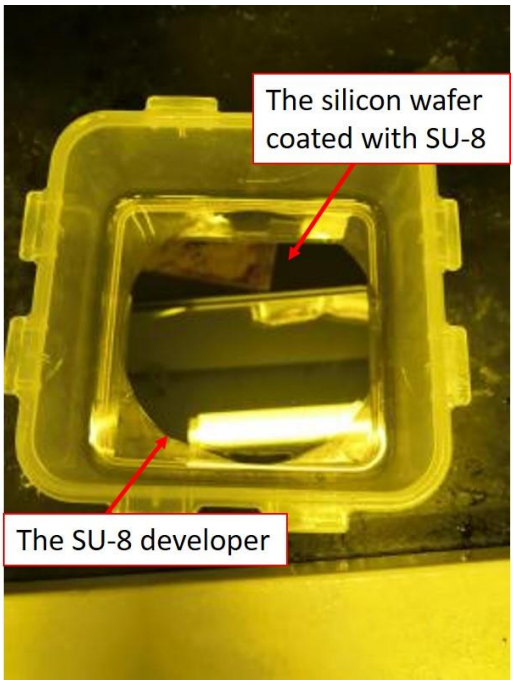

Fig. 5.3. SU-8 developer bath for the development of the silicon wafer after the post-exposure bake.

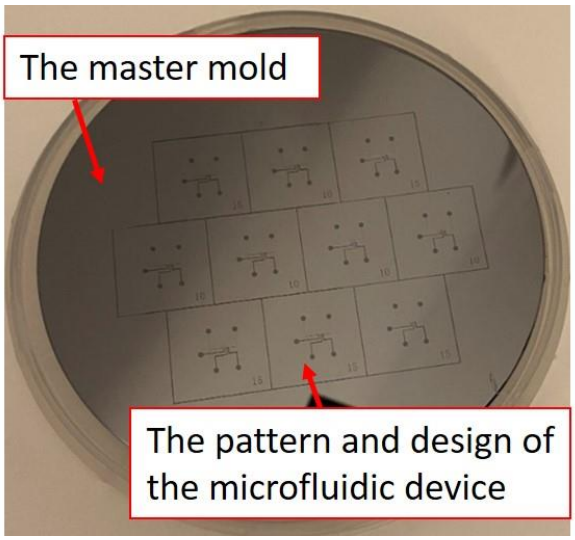

Fig. 5.4. The master mold that has 10 pieces of the device.

Step 5: making the channels and the membranes

First, the curing agent and the Sylgard 184 silicone elastomer, which were used to make PDMS with the weight ratio of 1:10, were mixed for 15 minutes. Second, the mixed PDMS was poured into the master mold. After that, the silicon wafer covered with mixed PDMS was put into a vacuum dryer (PC-3 plastic Vacuum Dryer, ZHONGXINQIHENG-cchip, China) so that the air bubbles in the PDMS could be removed. Then, the whole system was put into a drying oven (BPG-9056A, SHANGHAI BLUEPARD INSTRUMENTS CO., LTD, China) to cure the PDMS with a curing temperature of 85℃ and curing time of 20 minutes. Finally, the PDMS was peeled off from the master mold and was cut into 10 pieces. Besides, the inlets and outlets of the device were made by a hole punch.

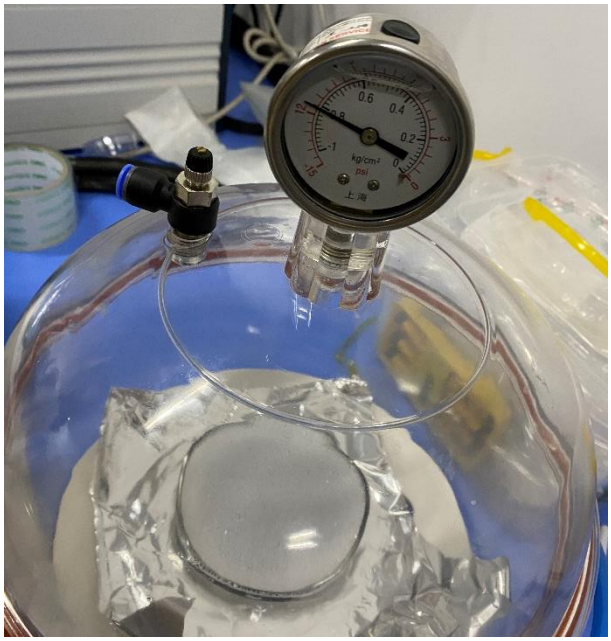

Fig. 5.5. The vacuum chamber that was used to remove the air bubbles in the PDMS.

5.4 Assembly

The PDMS with membranes and channels was bonded with a glass plate with a size of 75×25×1mm via the oxygen plasma machine (PDC-MG, ZHONGXINQIHENG-cchip, China) in Fig. 5.6. After bonding, the whole device was placed in the oven with a temperature of 85 ℃ for 2 hours to enhance the bonding strength. Fig. 5.7 presents the results of the device after the bonding process.

Fig. 5.6. The oxygen plasma applied to bond the PDMS with the glass.

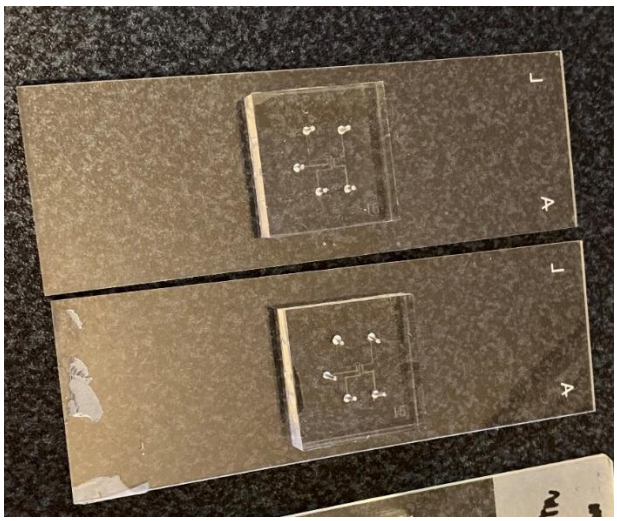

Fig. 5.7. Two pieces of PDMS devices after bonding process.

5.5 Conclusions

This chapter showed the fabrication process for the device designed in Chapter 3, which is based on photolithography and soft lithography. PDMS was applied due to its good cell compatibility, adequate Young's modulus, and low expense. One limitation of the device fabricated via soft lithography was that the thickness of the membrane could not be less than 10μm; otherwise, the membrane would be broken when peeling the PDMS off from the master mold. In other words, the limit of the membrane in terms of thickness with the fabrication process employed is 10μm.

Chapter 6: Experimentation

6.1 Introduction

This chapter will focus on the experiments to test the feasibility of the expected functions of the device to perform the pumping, particle sorting, and mixing functions in an integrated manner. The deflection of the membrane was examined to see whether it fulfills the required deflection (see the previous discussion in Fig. 4.6 and Table 4.1 in Chapter 4). The experiments were conducted on the fabricated PDMS device (in Fig. 5.7 in Chapter 5). Section 6.2 presents the preparation of samples with different microbeads. Section 6.3 presents the experiment setup. Section 6.4 shows the experimental results with discussions. The conclusion is presented in Section 6.5.

6.2 Sample preparation

The microbeads were used to mimic the cellular activities: i.e., circulating tumor cells (CTCs) being separated from the blood sample based on the principle of the difference in cell size and cell deformability. Polymer microbeads have been widely applied in the field of biomedical sciences, and have been produced to mimic the size and mechanical properties of cells [80].

Three types of microbeads with the diameters of 15 μm (1.2 g/cm^3,1 wt%, 10 ml, polymethyl methacrylate), 3 μm (~1.05 g/cm^3,1 wt%, 10 ml, Polystyrene), and 200 nm (~1.05 g/cm^3,1 wt%, 10 ml, Polystyrene) were purchased from Rigor Science. Microbeads with a diameter of 15 μm and 3 μm were used to mimic circulating tumor cells and normal blood cells, respectively. Microbeads with a diameter of 200 nm were used to take the place of the anti-cancer drugs. Based on the characteristics of the microbeads, 75% ethanol solution was used to avoid deposition and gathering of the microbeads. Both the preparation and experiment were conducted with a room temperature of 23-24℃, and a humidity of 60%.

Sample A was prepared by adding 1 μl PMMA microbeads with the diameter of 15 μm and 5 μl PS microbeads with the diameter of 3 μm into 10 ml 75% ethanol solution. Sample B was prepared by mixing10 μl PS microbeads with a diameter of 200 nm with 10 ml 75% ethanol solution.

6.3 Experiment setup

The visualizations of the behaviors of microbeads with the diameter of 15 μm and 3 μm after injecting into the device and the deflection of the membranes were completed on the inverted microscope (Nikon ECLIPSE Ti2, Nikon). The images were acquired through the software NIS-Elements which connected to the microscope. The microfluidic device was positioned on the plate holder, as shown in Fig. 6.1.

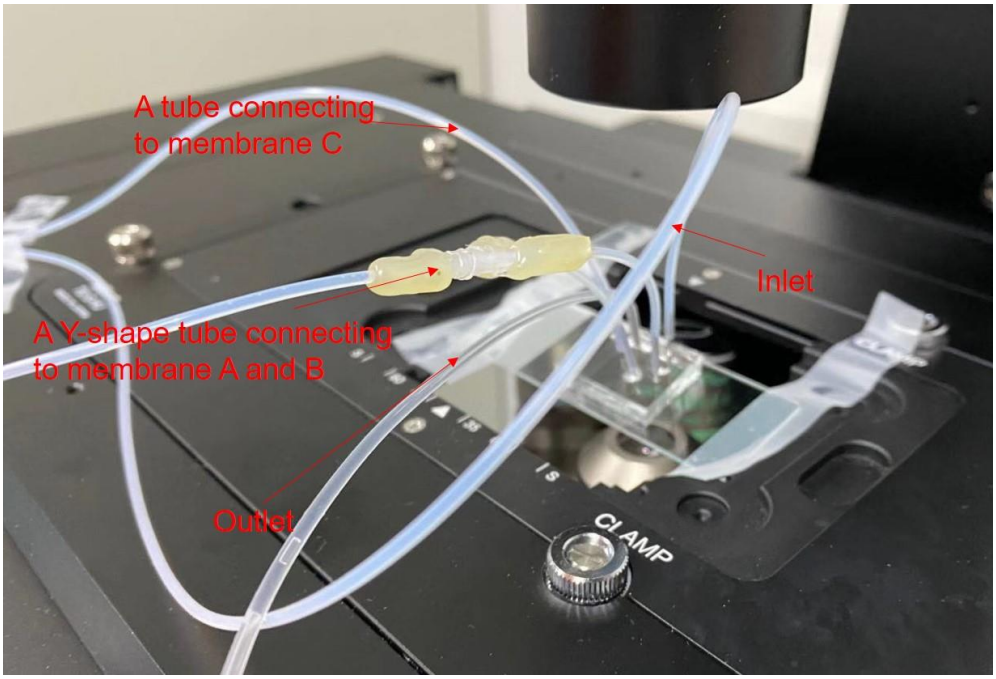

Fig. 6.1. The position of the microfluidic device.

Figure 6.2 is the schematic diagram of the system. Three 5-ml syringes were employed. Two of them were used to inject samples A and B into the microfluidic device, respectively. The other 5-ml syringe was used to pump water into and out of the chamber A and B in Fig. 6.2 through a Y-shape tube. Based on the validation described in Section 4.5, the

deflection of the membrane with a thickness of 10 μm, a length of 300 μm, the boundary load of 5828.71 mbar, was 24.4 μm by injecting gas into the chamber which is connected to the membrane. Gas is more compressible than water, so with the same volume and injection time, water can help to provide a higher boundary pressure on the membrane than gas. Water was applied to provide the boundary pressure. One 1-ml syringe was used to injecting water into the chamber C in Fig. 6.2. Two types of micropumps were employed to assist the injecting process. One type was the Pump 11 Pico Plus Elite micropumps (Pump 11 Pico Plus Elite series, Harvard Apparatus, America) which were applied to inject the sample to the main channel and inject water into the chamber C (see Fig. 6.2), respectively. The other type was the Biotaor micropump (RSP01-BG2, Biotaor instrument, China), which was used to inject water into the chambers of the deformable membranes A and B in Fig. 6.2. Fig. 6.3 is the set up of the whole system. The PTFE tubing was used to connect the device with the syringes.

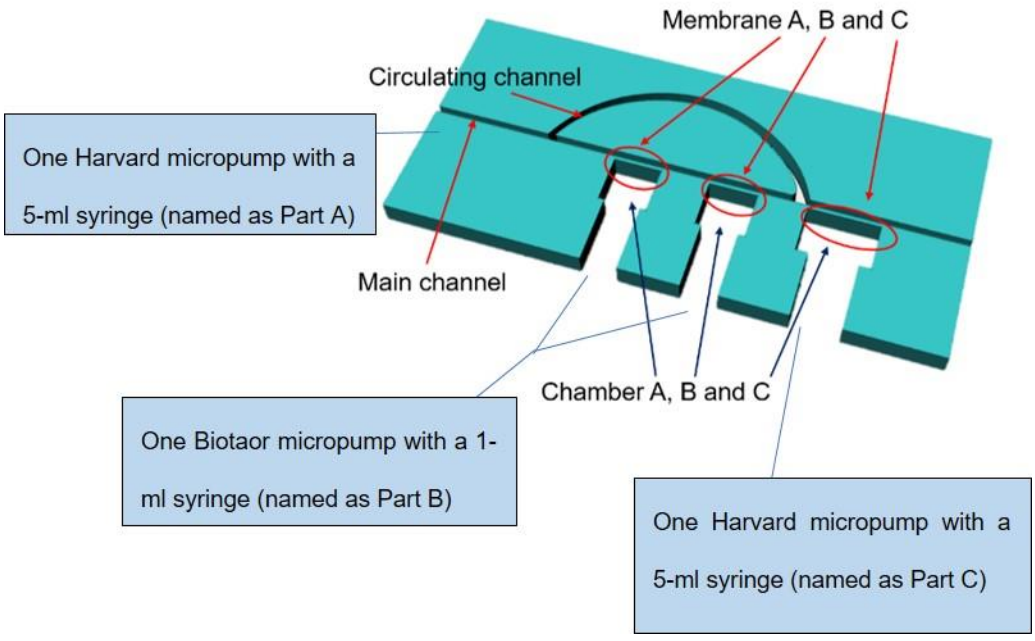

Fig. 6.2. The schematic diagram of the system.

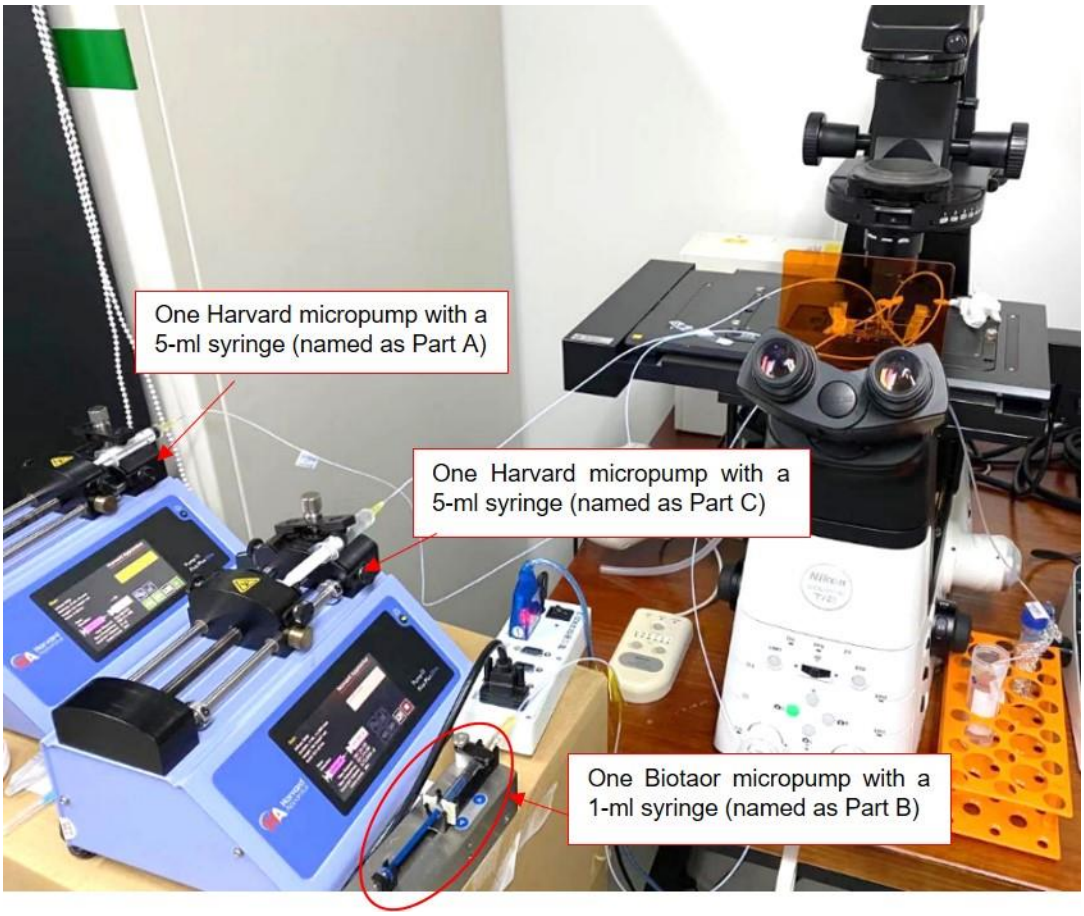

Fig. 6.3. The setup of the microfluidic system.

6.4 Experiment procedure along with results

At first, the microbeads with the diameter of 15 μm and 3 μm were sorted and separated. The microbeads with a diameter of 15 μm remained in the device, while the microbeads with a diameter of 3 μm flowed into the outlet. This step was designed to mimic the separation of the CTCs from normal blood cells.

Then, the selected microbeads with a diameter of 15 μm were mixed with microbeads with a diameter of 200 nm. This step was designed to mimic the mixing of CTCs with anti-cancer drugs. The 5-ml syringe filled with sample A was placed on the Harvard micropump and connected to the inlet of the microfluidic device. The other two syringes (one 5-ml syringe and one 1-ml syringe) filled with water were placed on the other two

micropump (one Harvard micropump, and one Biotaor micropump) and connected to the chambers to help with the membrane deflection. The outlet was connected to a collection tube.

Particle separation:

Step 1: The deflection of membrane C

First, the Harvard micropump with the 5-ml syringe filled with water was turned on to make the membrane C deflect. The micropump was not turned off until the deflected membrane stays at the position, as shown in Fig. 6.4, where only the microbeads with a diameter of 3 μm could pass through and flow to the outlet, and the microbeads with the diameter of 15 μm could not pass.

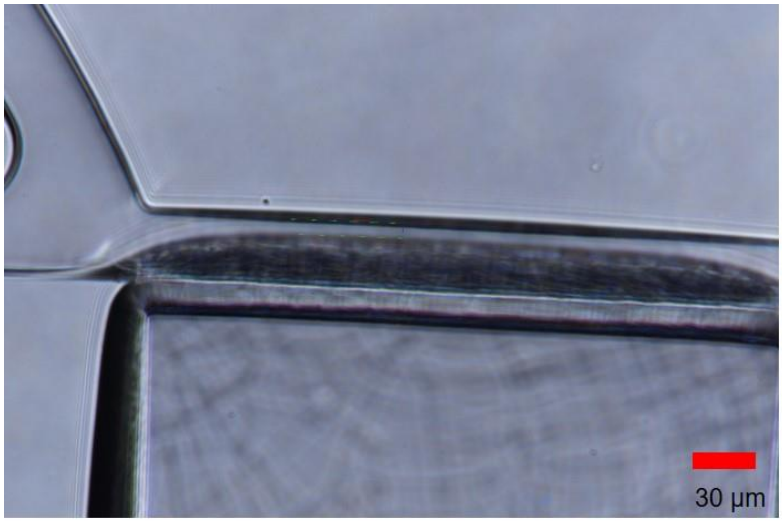

Fig. 6.4. The deflecting position of Membrane C.

Step 2: Injecting sample A

To avoid the deposition of the microbeads in the syringe and the tubes, the Ultrasonic Oscillation was applied. Then, the sample A (the mixture of microbeads with the diameter of 15 μm and 3 μm) with a volume of 5 ml was injected into the main channel with an

infusion speed of 0.5 ul/min. Microbeads with diameter of 15 μm were stuck and remained in the main channel, as shown in Fig. 6.5. When the injection was completed, the bigger size of microbeads with a diameter of 15 μm remained in the main channel as well as the circulating channel while the microbeads with a diameter of 3 μm flowed to the outlet of the device.

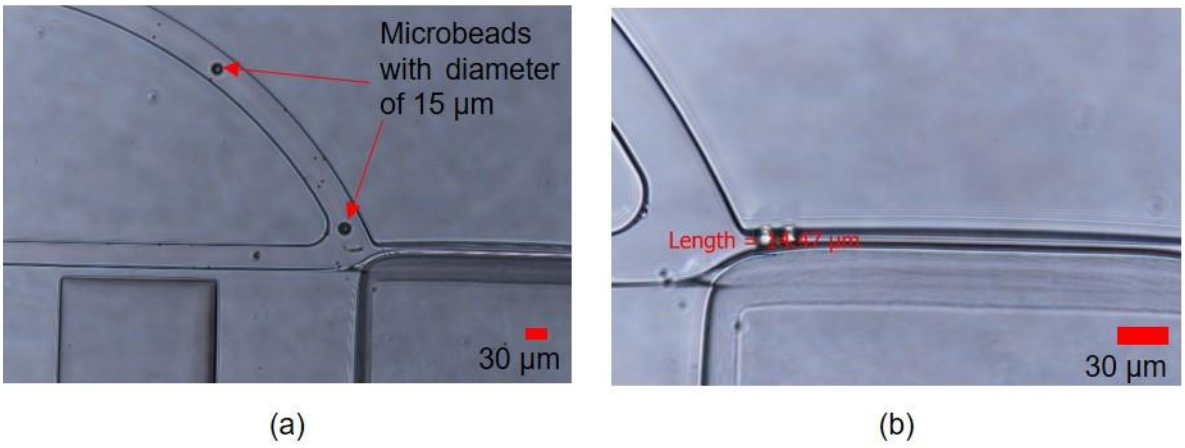

Fig. 6.5. The injection and sorting process of the microbeads (Sample A).

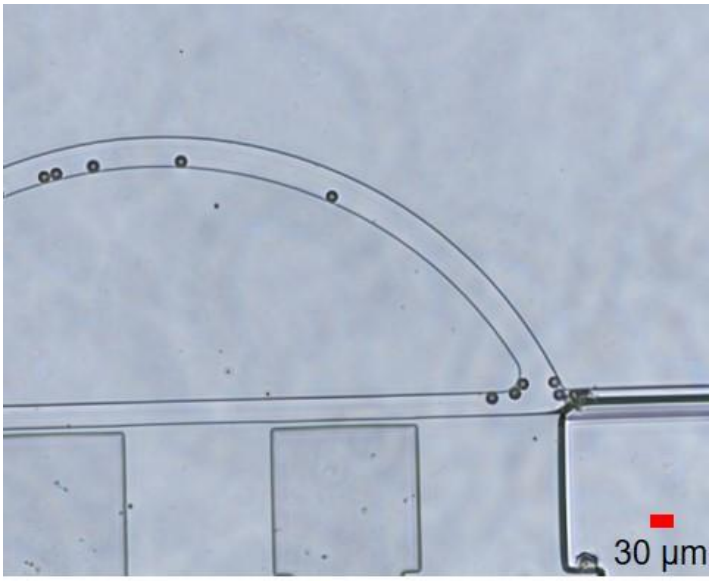

Fig. 6.6. The completion of particle separation.

Before proceeding to the next step, the selected microbeads with a diameter of 15 μm remained in the device, as shown in Fig. 6.6. Based on the experiments above, the particle sorting and separating function with the device developed was achieved.

Particle mixing:

Step 3: Injecting sample B

To avoid the deposition of the microbeads in the syringe and the tubes, an Ultrasonic Oscillation was applied. When the injection of sample A was completed, sample B (the mixture of microbeads with a diameter of 200 nm) with a volume of 5 ml was injected into the inlet of the same device with an infusion speed of 5 μl/min. Because of the resolution of the microscope (Nikon ECLIPSE Ti2, Nikon), the microbeads with diameter of 200 nm could not be seen. When the injection of sample B was completed, the Biotaor micropump, which was connected to the membrane A and B via a Y-shape tube, was turned on, so that the membrane A and B moved up and down to help with the mixing process, as shown in Fig. 6.7 (a) and Fig. 6.7(b).

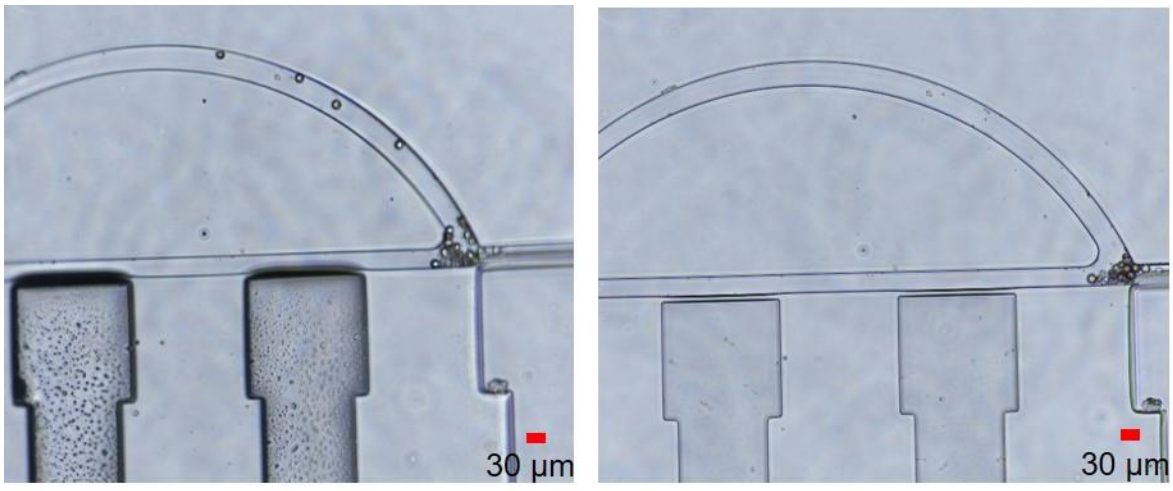

Fig. 6.7. The injection of sample B.

When the injection of sample B was completed, the selected microbeads were gathered, as shown in Fig. 6.7 (b). Then, turn off the micropump which is connected to the membranes A and B. The pressure within the device was gradually released to room pressure, as shown in Fig. 6.8. Then, turn off the micropump which is connected to membrane C. The selected microbeads with a diameter of 15 μm remained in the device after mixing with the microbeads with a diameter of 200 nm.

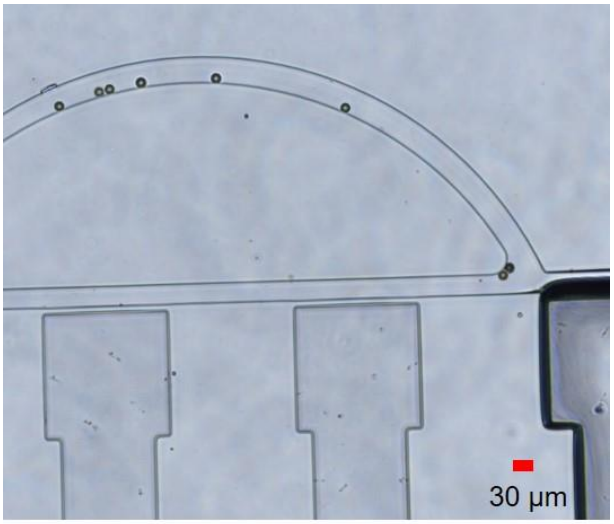

Fig. 6.8. Microbeads distribution after releasing the pressure within the device to room pressure.

According to Section 3.3, the active stirrer, long mixing path and long residence time could help to enhance the mixing efficiency. For this study, the deflection of the membranes A and B acted as the active stirrer, and the deflection of the membrane C helped the selected microbeads to stay in the device to have a long residence time to mix with the microbeads with the diameter of 200 nm. The microfluidic device was designed in Chapter 4 to have a long mixing path. Based on the discussion above, the mixing of the particles with the diameter of 15 μm and 200 nm was achieved.

6.5 Conclusions

In this chapter, the experiments were presented. The deflections of the membranes met the requirements of the design to close the main channel partially. The motions of the microbeads with the diameter of 15 μm and 3 μm were observed to validate the particle sorting functions. However, because of the resolution of the microscope, the particle with a diameter of 200 nm could not been seen. Due to the factors to enhance the mixing efficiency, the mixing function could be fulfilled based on the design of the microfluidic device. The pumping functions were restricted to observing whether there were deflections of the membranes A and B because of the limitation of the resolution of the microscope Nikon (ECLIPSE Ti2, Nikon).

The experimental results show that the particle sorting and separating functions can be achieved by the device. The mixing function of this device can be achieved and enhanced according to Section 3.3 that the active stirrer, long mixing path, and long residence time can help to enhance the mixing efficiency. The pumping function of the microfluidic device was also accomplished because of the deflection of the membranes A and B. But due to the resolution of the microscope (Nikon ECLIPSE Ti2, Nikon), the distribution of the microbeads with a diameter of 200nm could not be observed. In conclusion, the experiments partially proved that the device can effectively perform an integrated function of (circular) pumping, mixing and separating.

Chapter 7: Conclusions and Recommendations for Future Work

7.1 Overview and conclusion

Microfluidics is a subject of knowledge about fluid circuits. Microfluidic technology allows us to develop devices to manipulate a small volume of fluids to flow within the device in microscale or nanoscale. The generic manipulation includes pumping, separating, and mixing. Currently, one function is played at one time by one device logically. With the desire to make a human-made natural environment for cell, tissue, organ, manipulation of these functions simultaneously or without an artifact in terms of time and place is required, and this is a promising research area for the future.

This thesis was motivated by the above observation and was designed as a piolet step in this research area. The thesis was designed to attempt to develop a device to integrate the three generic functions. Further, the thesis took CTCs as an application background to shape the research to be readily useful to applications. Therefore, the overall objective of the thesis was to develop a microfluidic device to test its feasibility to perform the pumping, particle separating, and particle mixing functions simultaneously and continuously. The specific objectives are re-visited herein:

1. to design a microfluidic device for integration of the functions of pumping, particle sorting, and particle mixing, performed simultaneously with the possibility that the device being fabricated with the current micro-fabrication techniques.
2. to compare the lithography-based approach and the 3D printing approach to fabrication of the designed device to explore the limit of the design and fabrication.
3. to build the test apparatus including the device as designed in Objective 1 along with other instruments, and to test whether the expected functions of the device can be achieved along with its performance.

Overall, this thesis has demonstrated the feasibility of the device to perform the three generic functions simultaneously and continuously. That is to say, the overall objective is

achievable. The research activities were carried out, including design of the device by employing general design theories and methodologies, such as Axiomatic Design Theory (in Chapter 3), simulation with a multi-phase physics software system called COMSOL (in Chapter 4), fabrication by a combined photolithography and soft lithography approach (in Chapter 5), and testing (in Chapter 6).

The main conclusion drawn from the work of this thesis are: (1) the design of the microfluidic device with the elastically deformable membrane concept can readily achieve the simultaneous performing of the three generic functions (pumping, mixing, and separating); (2) the fabrication technology which combines the photolithography and soft-lithography can achieve the thickness of the membrane to be about 10 microns; (3) the deflection of the membrane as fabricated with its thickness greater than 10 microns is sufficient to make the device effective to its intended function.

7.2 Contributions

In the field of microfluidics, especially microfluidic device technology, the device as designed and fabricated is novel to the best of the author's knowledge. Existing devices may be used to perform more than one function but there is distinct time stamp to each of the functions, and there is unnecessary transportation between each function unit. In the field of biomedical engineering, in particular this thesis provides a proof that the size- and deflection-based principle to separate two groups of particles, CTCs from the blood stream in this case, is effective. Subsequently, it is promising to further shape it to a practically viable device for separation of CTCs from the blood stream.

7.3 Limitations

There are several limitations to this work. The first limitation is the restriction of the fabrication facility available to fabricate the microfluidic device. The fabrication of the device was based on soft lithography. When fabricating the membrane with a thickness of 5 um, the PDMS membrane could not be easily peeled off from the master mold, and

it was broken all the time. When applying the 3D printing method, Two-photo polymerization (Nanoscribe GmbH, Karlsruhe, Germany), the resolution of the 3D printer was too small to print the device with the device size in microscale. So, the thickness of the membrane turned out to be 10 μm only in this thesis.

The second limitation is the restriction of the microscope with a resolution of 1 μm. Microbeads with the diameter of 200 nm was applied to mimic the anticancer drug; however, because of the resolution of the microscope, the microbeads with the diameter of 200 nm could not be observed, which would lead to the inability to observe the distribution of the microbeads with the diameter of 200 nm after mixing and pumping process.

The third limitation is the application of microbeads. The deposition of the microbeads within the sample injecting syringes and plastic tubing may lead to the consumption of the sample.

The fourth limitation is the simulation tool. The computing facility is not enough to simulate the whole system. Only the membrane of the system is simulated. Fortunately, due to the working principle and design of the device, the simulation of the deformable membranes does not compromise the result.

7.4 Future work

Several recommendations for future work are made. First, the fabrication of the membrane can be completed via 3D printing method to explore the limitation of the design (i.e., membrane thickness, channel size). A smaller membrane thickness and channel size are expected via 3D printers of which the resolution can fulfill the design requirements to print the device in microscale. Second, in-vitro experiments may need to be conducted to test the performance of the novel multifunctional device by applying standard blood cell samples to take the place of the microbeads in this case. Third, other materials than PDMS may be applied to fabricate the microfluidic device to explore the deformability of

the membrane. Fourth, the observation of the distribution of microbeads with diameter in nanoscale in the device can be seen via fluorescence imaging technique. Then, the mechanical properties of different microbeads need to be studied to verify the compliance of CTCs and normal blood cells. Finally, the membranes A and B may be designed larger than what it is designed now to increase the scope of its deflection for a wider scope of applications.

References

[1] N.-T. Nguyen and Z. Wu, "Micromixers—a review," *Journal of Micromechanics and Microengineering,* vol. 15, no. 2, p. R1, 2004.

[2] H. A. Stone, A. D. Stroock, and A. Ajdari, "Engineering flows in small devices: microfluidics toward a lab-on-a-chip," *Annual Review of Fluid Mechanics,* vol. 36, pp. 381-411, 2004.

[3] A. Farahinia, W. Zhang, and I. Badea, "Novel Microfluidic Approaches to Circulating Tumor Cell Separation and Sorting of Blood Cells: A Review," *Journal of Science: Advanced Materials and Devices,* 2021.

[4] P. Abgrall and A. Gue, "Lab-on-chip technologies: making a microfluidic network and coupling it into a complete microsystem—a review," *Journal of Micromechanics and Microengineering,* vol. 17, no. 5, p. R15, 2007.

[5] Y.-N. Wang and L.-M. Fu, "Micropumps and biomedical applications–A review," *Microelectronic Engineering,* vol. 195, pp. 121-138, 2018.

[6] F. Zheng, F. Fu, Y. Cheng, C. Wang, Y. Zhao, and Z. Gu, "Organ‐on‐a‐Chip Systems: microengineering to biomimic living systems," *Small,* vol. 12, no. 17, pp. 2253-2282, 2016.

[7] Z. Bi, Y. Lin, and W. Zhang, "The general architecture of adaptive robotic systems for manufacturing applications," *Robotics and Computer-Integrated Manufacturing,* vol. 26, no. 5, pp. 461-470, 2010.

[8] W. Zhang and J. Wang, "Design theory and methodology for enterprise systems," *Enterprise Information Systems,* vol. 10, no. 3, pp. 245-248, 2016.

[9] S. Herrlich, S. Spieth, S. Messner, and R. Zengerle, "Osmotic micropumps for drug delivery," *Advanced drug delivery reviews,* vol. 64, no. 14, pp. 1617-1627, 2012.

[10] F. E. Tay, *Microfluidics and BioMEMS applications*. Springer, 2002.

[11] A. Nisar, N. Afzulpurkar, B. Mahaisavariya, and A. Tuantranont, "MEMS-based micropumps in drug delivery and biomedical applications," *Sensors and Actuators B: Chemical,* vol. 130, no. 2, pp. 917-942, 2008.

[12] M. M. Said, J. Yunas, B. Bais, A. A. Hamzah, and B. Y. Majlis, "Hybrid polymer composite membrane for an electromagnetic (EM) valveless micropump," *Journal of Micromechanics and Microengineering,* vol. 27, no. 7, p. 075027, 2017.

[13] G. Cai, L. Xue, H. Zhang, and J. Lin, "A review on micromixers," *Micromachines,* vol. 8, no. 9, p. 274, 2017.

[14] T. Bayraktar and S. B. Pidugu, "Characterization of liquid flows in microfluidic systems," *International Journal of Heat and Mass Transfer,* vol. 49, no. 5-6, pp. 815-824, 2006.

[15] A. Affanni and G. Chiorboli, "Development of an enhanced MHD micromixer based on axial flow modulation," *Sensors and Actuators B: Chemical,* vol. 147, no. 2, pp. 748-754, 2010.

[16] C.-Y. Lee and L.-M. Fu, "Recent advances and applications of micromixers," *Sensors and Actuators B: Chemical,* vol. 259, pp. 677-702, 2018.

[17] K. Ward and Z. H. Fan, "Mixing in microfluidic devices and enhancement methods," *Journal of Micromechanics and Microengineering,* vol. 25, no. 9, p. 094001, 2015.

[18] V. Hessel, H. Löwe, and F. Schönfeld, "Micromixers—a review on passive and active mixing principles," *Chemical Engineering Science,* vol. 60, no. 8-9, pp. 2479-2501, 2005.

[19] X. Jiang, Q. Xu, S. K. Dertinger, A. D. Stroock, T.-m. Fu, and G. M. Whitesides, "A general method for patterning gradients of biomolecules on surfaces using microfluidic networks," *Analytical chemistry,* vol. 77, no. 8, pp. 2338-2347, 2005.

[20] K. Anwar, T. Han, S. Yu, and S. M. Kim, "Integrated micro/nano-fluidic system for mixing and preconcentration of dissolved proteins," *Microchimica Acta,* vol. 173, pp. 331-335, 2011.

[21] D. Kim, H. Oh, T. Park, J. Choo, and S. H. Lee, "An easily integrative and efficient micromixer and its application to the spectroscopic detection of glucose-catalyst reactions," *Analyst,* vol. 130, no. 3, pp. 293-298, 2005.

[22] Y. Han, J.-J. Wang, X.-P. Gu, and L.-F. Feng, "Numerical simulation on micromixing of viscous fluids in a stirred-tank reactor," *Chemical Engineering Science,* vol. 74, pp. 9-17, 2012.

[23] J. Morsbach, A. H. Müller, E. Berger-Nicoletti, and H. Frey, "Living polymer chains with predictable molecular weight and dispersity via carbanionic polymerization in continuous flow: Mixing rate as a key parameter," *Macromolecules,* vol. 49, no. 14, pp. 5043-5050, 2016.

[24] N. Y. Lee, M. Yamada, and M. Seki, "Development of a passive micromixer based on repeated fluid twisting and flattening, and its application to DNA purification," *Analytical and bioanalytical chemistry,* vol. 383, no. 5, pp. 776-782, 2005.

[25] M. X. Lin *et al.*, "Continuous labeling of circulating tumor cells with microbeads using a vortex micromixer for highly selective isolation," *Biosensors and Bioelectronics,* vol. 40, no. 1, pp. 63-67, 2013.

[26] K. Y. Lee, S. Park, Y. R. Lee, and S. K. Chung, "Magnetic droplet microfluidic system incorporated with acoustic excitation for mixing enhancement," *Sensors and actuators A: Physical,* vol. 243, pp. 59-65, 2016.

[27] D. Zou and D. Cui, "Advances in isolation and detection of circulating tumor cells based on microfluidics," *Cancer biology & medicine,* vol. 15, no. 4, p. 335, 2018.

[28] S.-J. Hao, Y. Wan, Y.-Q. Xia, X. Zou, and S.-Y. Zheng, "Size-based separation methods of circulating tumor cells," *Advanced Drug Delivery Reviews,* vol. 125, pp. 3-20, 2018.

[29] P. Preira, V. Grandne, J.-M. Forel, S. Gabriele, M. Camara, and O. Theodoly, "Passive circulating cell sorting by deformability using a microfluidic gradual filter," *Lab on a Chip,* vol. 13, no. 1, pp. 161-170, 2013.

[30] W. J. Allard *et al.*, "Tumor cells circulate in the peripheral blood of all major carcinomas but not in healthy subjects or patients with nonmalignant diseases," *Clinical cancer research,* vol. 10, no. 20, pp. 6897-6904, 2004.

[31] Y. Dong *et al.*, "Microfluidics and circulating tumor cells," *The Journal of Molecular Diagnostics,* vol. 15, no. 2, pp. 149-157, 2013.

[32] K. Ino *et al.*, "Cell culture arrays using magnetic force-based cell patterning for dynamic single cell analysis," *Lab on a Chip,* vol. 8, no. 1, pp. 134-142, 2008.

[33] T. Henighan *et al.*, "Manipulation of magnetically labeled and unlabeled cells with mobile magnetic traps," *Biophysical Journal,* vol. 98, no. 3, pp. 412-417, 2010.

[34] A. Chen *et al.*, "On-chip magnetic separation and encapsulation of cells in droplets," *Lab on a Chip,* vol. 13, no. 6, pp. 1172-1181, 2013.

[35] K. Lee, Y. Yi, and Y. Yu, "Remote control of T cell activation using magnetic Janus particles," *Angewandte Chemie International Edition,* vol. 55, no. 26, pp. 7384-7387, 2016.

[36] J. Voldman, M. L. Gray, M. Toner, and M. A. Schmidt, "A microfabrication-based dynamic array cytometer," *Analytical chemistry,* vol. 74, no. 16, pp. 3984-3990, 2002.

[37] Z. Zhu, O. Frey, D. S. Ottoz, F. Rudolf, and A. Hierlemann, "Microfluidic single-cell cultivation chip with controllable immobilization and selective release of yeast cells," *Lab on a Chip,* vol. 12, no. 5, pp. 906-915, 2012.

[38] M. Kobayashi, S. H. Kim, H. Nakamura, S. Kaneda, and T. Fujii, "Cancer cell analyses at the single cell-level using electroactive microwell array device," *PloS One,* vol. 10, no. 11, p. e0139980, 2015.

[39] X. Guo and R. Zhu, "Controllably moving individual living cell in an array by modulating signal phase difference based on dielectrophoresis," *Biosensors and Bioelectronics,* vol. 68, pp. 529-535, 2015.

[40] Y. Shen, Z. Song, Y. Yan, Y. Song, X. Pan, and Q. Wang, "Automatic and selective single cell manipulation in a pressure-driven microfluidic lab-on-chip device," *Micromachines,* vol. 8, no. 6, p. 172, 2017.

[41] X. Gou, R. Wang, S. S. Lam, J. Hou, A. Y. Leung, and D. Sun, "Cell adhesion manipulation through single cell assembly for characterization of initial cell-to-cell interaction," *Biomedical Engineering Online,* vol. 14, no. 1, p. 114, 2015.

[42] X. Wang *et al.*, "Enhanced cell sorting and manipulation with combined optical tweezer and microfluidic chip technologies," *Lab on a Chip,* vol. 11, no. 21, pp. 3656-3662, 2011.

[43] M. Tardif *et al.*, "Single-cell bacterium identification with a SOI optical microcavity," *Applied Physics Letters,* vol. 109, no. 13, p. 133510, 2016.

[44] P. Chen, X. Feng, W. Du, and B.-F. Liu, "Microfluidic chips for cell sorting," *Frontiers in Bioscience,* vol. 13, pp. 2464-2483, 2008.

[45] A. Ahmad Khalili, M. R. Ahmad, M. Takeuchi, M. Nakajima, Y. Hasegawa, and R. Mohamed Zulkifli, "A microfluidic device for hydrodynamic trapping and manipulation platform of a single biological cell," *Applied Sciences,* vol. 6, no. 2, p. 40, 2016.

[46] Y. Zhou *et al.*, "A microfluidic platform for trapping, releasing and super-resolution imaging of single cells," *Sensors and Actuators B: Chemical,* vol. 232, pp. 680-691, 2016.

[47] M. Chabert and J.-L. Viovy, "Microfluidic high-throughput encapsulation and hydrodynamic self-sorting of single cells," *Proceedings of the National Academy of Sciences,* vol. 105, no. 9, pp. 3191-3196, 2008.

[48] F. Guo *et al.*, "Three-dimensional manipulation of single cells using surface acoustic waves," *Proceedings of the National Academy of Sciences,* vol. 113, no. 6, pp. 1522-1527, 2016.

[49] X. Ding *et al.*, "On-chip manipulation of single microparticles, cells, and organisms using surface acoustic waves," *Proceedings of the National Academy of Sciences,* vol. 109, no. 28, pp. 11105-11109, 2012.

[50] A. Barani *et al.*, "Microfluidic integrated acoustic waving for manipulation of cells and molecules," *Biosensors and Bioelectronics,* vol. 85, pp. 714-725, 2016.

[51] Y. Song, M. Li, X. Pan, Q. Wang, and D. Li, "Size‐based cell sorting with a resistive pulse sensor and an electromagnetic pump in a microfluidic chip," *Electrophoresis,* vol. 36, no. 3, pp. 398-404, 2015.

[52] Z. Song, M. Li, B. Li, Y. Yan, and Y. Song, "Automatic detecting and counting magnetic beads‐labeled target cells from a suspension in a microfluidic chip," *Electrophoresis,* vol. 40, no. 6, pp. 897-905, 2019.

[53] D. V. Polniak, E. Goodrich, N. Hill, and B. H. Lapizco-Encinas, "Separating large microscale particles by exploiting charge differences with dielectrophoresis," *Journal of Chromatography A,* vol. 1545, pp. 84-92, 2018.

[54] A. Fadl, S. Demming, Z. Zhang, S. Büttgenbach, M. Krafczyk, and D. M. Meyer, "A multifunction and bidirectional valve-less rectification micropump based on bifurcation geometry," *Microfluidics and Nanofluidics,* vol. 9, no. 2-3, pp. 267-280, 2010.

[55] H.-J. Kang and B. Choi, "Development of the MHD micropump with mixing function," *Sensors and Actuators A: Physical,* vol. 165, no. 2, pp. 439-445, 2011.

[56] X. Xiao and C. N. Kim, "Numerical analysis of an MHD micro-device with simultaneous mixing and pumping capability," *Journal of Industrial and Engineering Chemistry,* vol. 38, pp. 23-36, 2016.

[57] H. Becker, "Hype, hope and hubris: the quest for the killer application in microfluidics," *Lab on a Chip,* vol. 9, no. 15, pp. 2119-2122, 2009.

[58] S. Waheed *et al.*, "3D printed microfluidic devices: enablers and barriers," *Lab on a Chip,* vol. 16, no. 11, pp. 1993-2013, 2016.

[59] K. G. Lee *et al.*, "3D printed modules for integrated microfluidic devices," *RSC Advances,* vol. 4, no. 62, pp. 32876-32880, 2014.

[60] A. K. Au, W. Huynh, L. F. Horowitz, and A. Folch, "3D ‐ printed microfluidics," *Angewandte Chemie International Edition,* vol. 55, no. 12, pp. 3862-3881, 2016.

[61] A. Mazzoli, "Selective laser sintering in biomedical engineering," *Medical & Biological Engineering & Computing,* vol. 51, no. 3, pp. 245-256, 2013.

[62] B. Duan and M. Wang, "Selective laser sintering and its application in biomedical engineering," *MRS Bulletin,* vol. 36, no. 12, pp. 998-1005, 2011.

[63] M.-T. Lee, D. Lee, A. Sherry, and C. P. Grigoropoulos, "Rapid selective metal patterning on polydimethylsiloxane (PDMS) fabricated by capillarity-assisted laser direct write," *Journal of Micromechanics and Microengineering,* vol. 21, no. 9, p. 095018, 2011.

[64] (December 20). *Online material*. Available: http://www.custompartnet.com/wu/selective-laser-sintering

[65] T. Himmer, T. Nakagawa, and M. Anzai, "Lamination of metal sheets," *Computers in Industry,* vol. 39, no. 1, pp. 27-33, 1999.

[66] T. Obikawa, M. Yoshino, and J. Shinozuka, "Sheet steel lamination for rapid manufacturing," *Journal of Materials Processing Technology,* vol. 89, pp. 171-176, 1999.

[67] (November 21). *Online material*. Available: http://www.custompartnet.com/wu/laminated-object-manufacturing

[68] A. Rasouli, "An integrated continuous micro-fluidic switch valve," University of Saskatchewan, 2019.

[69] T. M. A. R. A. Layton, "Introductory MEMS: Fabrication and applications."

[70] C.-W. Tsao, "Polymer microfluidics: Simple, low-cost fabrication process bridging academic lab research to commercialized production," *Micromachines,* vol. 7, no. 12, p. 225, 2016.

[71] L. Fan, M. Cai, Y. Lin, and W. Zhang, "Axiomatic design theory: further notes and its guideline to applications," *International Journal of Materials and Product Technology,* vol. 51, no. 4, pp. 359-374, 2015.

[72] Z. Dai, "Improvement of general design theory and methodolgy with its application to design of a retractor for ventral hernia repair surgery," University of Saskatchewan, 2019.

[73] N. P. Suh, "Design of systems," *CIRP Annals,* vol. 46, no. 1, pp. 75-80, 1997.

[74] N. P. Suh and P. N. Suh, *The principles of design* (no. 6). Oxford University Press on Demand, 1990.

[75] D. D. Frey, E. Jahangir, and F. Engelhardt, "Computing the information content of decoupled designs," *Research in Engineering Design,* vol. 12, no. 2, pp. 90-102, 2000.

[76] W. Zhang, Y. Lin, and N. Sinha, "On the function-behavior-structure model for design," *Proceedings of the Canadian Engineering Education Association (CEEA),* 2005.

[77] W. Su, H. Yu, L. Jiang, W. Chen, H. Li, and J. Qin, "Integrated microfluidic device for enrichment and identification of circulating tumor cells from the blood of patients with colorectal cancer," *Disease Markers,* vol. 2019, p. 8945974, 2019.

[78] B.-h. Chueh, D. Huh, C. R. Kyrtsos, T. Houssin, N. Futai, and S. Takayama, "Leakage-free bonding of porous membranes into layered microfluidic array systems," *Analytical Chemistry,* vol. 79, no. 9, pp. 3504-3508, 2007.

[79] Y.-S. Yu and Y.-P. Zhao, "Deformation of PDMS membrane and microcantilever by a water droplet: Comparison between Mooney–Rivlin and linear elastic constitutive models," *Journal of Colloid and Interface Science,* vol. 332, no. 2, pp. 467-476, 2009.

[80] N. R. Labriola, E. Mathiowitz, and E. M. Darling, "Fabricating polyacrylamide microbeads by inverse emulsification to mimic the size and elasticity of living cells," *Biomaterials science,* vol. 5, no. 1, pp. 41-45, 2017.

Appendices:

A: Permission to reproduce content

Permission for Figure 2.2 and 2.3:

Dear Yongqin Yang

Thank you for your request to reproduce material published by IOP Publishing *in your thesis* ***"An integrated multi-functional microfluidic device with pumping, particle sorting, and mixing functions"*** *to be published by* ***University of Saskatchewan.***

Regarding:

- ***Figures 2 & 5*** *from* ***"Hybrid polymer composite membrane for an electromagnetic (EM) valveless micropump"***

We are happy to grant permission for the use you request on the terms set out below.

License to publish material published by IOP Publishing

Please provide the below to your new publisher as proof of permission.

Conditions

Non-exclusive, non-transferrable, revocable, worldwide, permission to use the material in print and electronic form will be granted **subject to the following conditions:**

- Permission will be cancelled without notice if you fail to fulfil any of the conditions of this letter.
- You will make reasonable efforts to contact the author(s) to seek consent for your intended use. Contacting one author acting expressly as authorised agent for their co-authors is acceptable.
- You will reproduce the following prominently alongside the material:
    - the source of the material, including author, article title, title of journal, volume number, issue number (if relevant), page range (or first page if this is the only information available) and date of first publication. This information can be contained in a footnote or reference note; or
    - a link back to the article (via DOI); and
    - **if practical and IN ALL CASES for works published under any of the Creative Commons licences the words "© IOP Publishing. Reproduced with permission. All rights reserved"**
- The material will not, without the express permission of the author(s), be used in any way which, in the opinion of IOP Publishing, could distort or alter the author(s)' original intention(s)

and meaning, be prejudicial to the honour or reputation of the author(s) and/or imply endorsement by the author(s) and/or IOP Publishing.

- Payment of £0 is received in full by IOP Publishing prior to use.

This permission does not apply to any material/figure which is credited to another source in our publication or has been obtained from a third party. Express permission for such materials/figures must be obtained from the copyright owner.

Special Conditions – For STM Signatories ONLY (as agreed as part of the STM Guidelines)

For content reuse requests that qualify for permission under the STM Permissions Guidelines, which may be updated from time to time, the STM Permissions Guidelines supplement the terms and conditions contained in this license.

Kind regards,

Sophie Milne

Copyright & Permissions Team

Sophie Milne - Rights & Permissions Assistant

Sophie Brittain - Rights & Permissions Assistant

Cameron Wood - Legal & Rights Adviser

Contact Details

E-mail: permissions@ioppublishing.org

For further information about copyright and how to request permission:

https://publishingsupport.iopscience.iop.org/copyright-journals/
See also:
https://publishingsupport.iopscience.iop.org/
Please see our Author Rights Policy
https://publishingsupport.iopscience.iop.org/author-rights-policies/
Please note: We do not provide signed permission forms as a separate attachment. Please print this email and provide it to your publisher as proof of permission. **Please note**: Any statements made by IOP Publishing to the effect that authors do not need to get permission to use any content where IOP Publishing is not the publisher is not intended to constitute any sort of legal advice. Authors must make their own decisions as to the suitability of the content they are using and whether they require permission for it to be published within their article.

Permission for Figure 2.4 and 2.5:

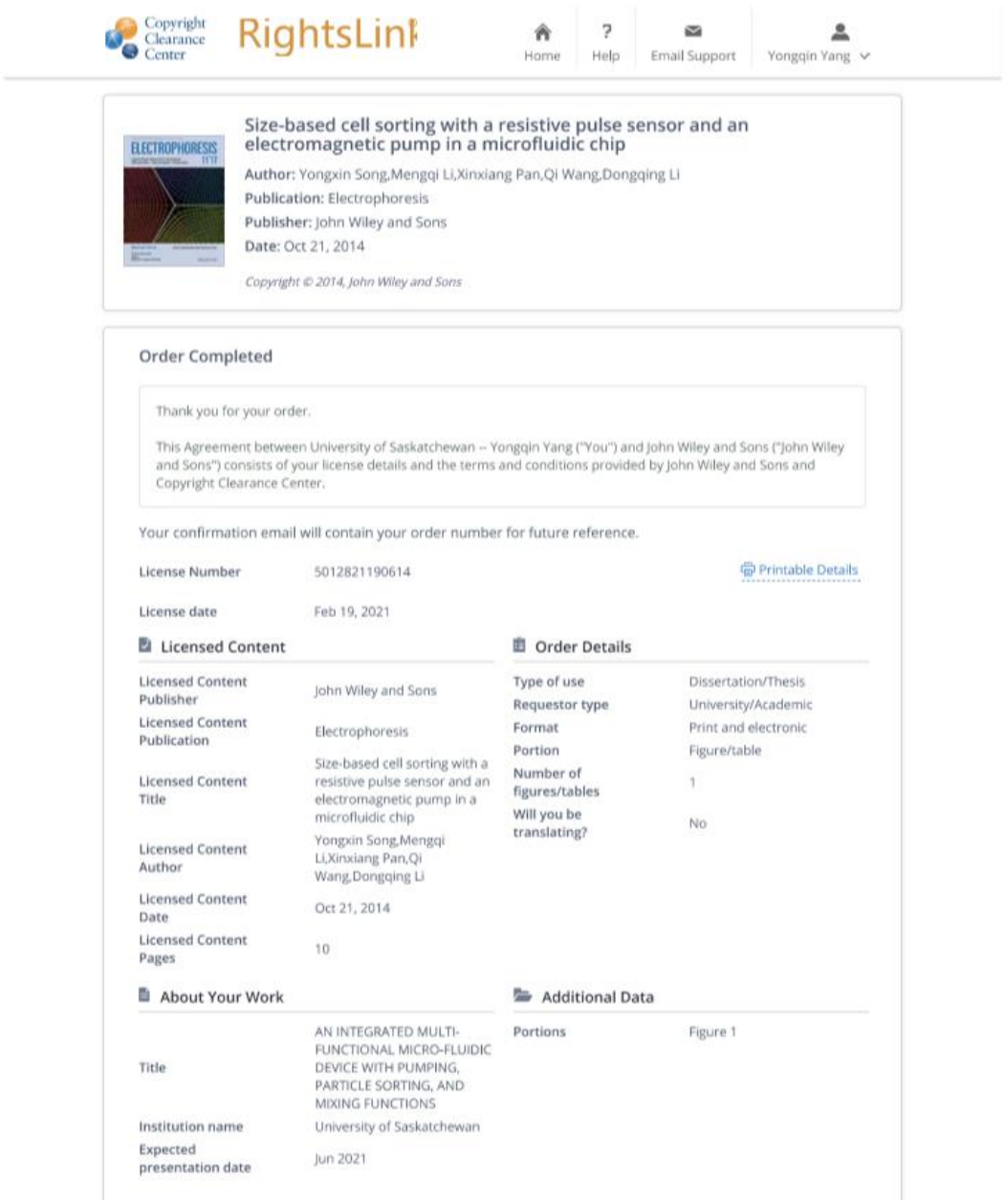

Copyright Clearance Center RightsLink

Home | Help | Email Support | Yongqin Yang

Size-based cell sorting with a resistive pulse sensor and an electromagnetic pump in a microfluidic chip

Author: Yongxin Song,Mengqi Li,Xinxiang Pan,Qi Wang,Dongqing Li
Publication: Electrophoresis
Publisher: John Wiley and Sons
Date: Oct 21, 2014

Copyright © 2014, John Wiley and Sons

Order Completed

Thank you for your order.

This Agreement between University of Saskatchewan -- Yongqin Yang ("You") and John Wiley and Sons ("John Wiley and Sons") consists of your license details and the terms and conditions provided by John Wiley and Sons and Copyright Clearance Center.

Your confirmation email will contain your order number for future reference.

Printable Details

License Number	5012821190614
License date	Feb 19, 2021

Licensed Content

Licensed Content Publisher	John Wiley and Sons
Licensed Content Publication	Electrophoresis
Licensed Content Title	Size-based cell sorting with a resistive pulse sensor and an electromagnetic pump in a microfluidic chip
Licensed Content Author	Yongxin Song,Mengqi Li,Xinxiang Pan,Qi Wang,Dongqing Li
Licensed Content Date	Oct 21, 2014
Licensed Content Pages	10

Order Details

Type of use	Dissertation/Thesis
Requestor type	University/Academic
Format	Print and electronic
Portion	Figure/table
Number of figures/tables	1
Will you be translating?	No

About Your Work

Title	AN INTEGRATED MULTI-FUNCTIONAL MICRO-FLUIDIC DEVICE WITH PUMPING, PARTICLE SORTING, AND MIXING FUNCTIONS
Institution name	University of Saskatchewan
Expected presentation date	Jun 2021

Additional Data

Portions	Figure 1

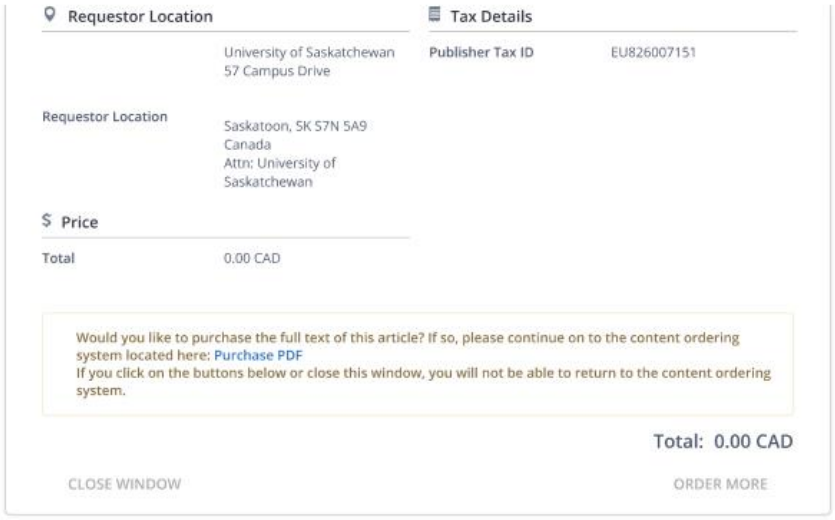

Permission for Figure 2.6 and 2.7:

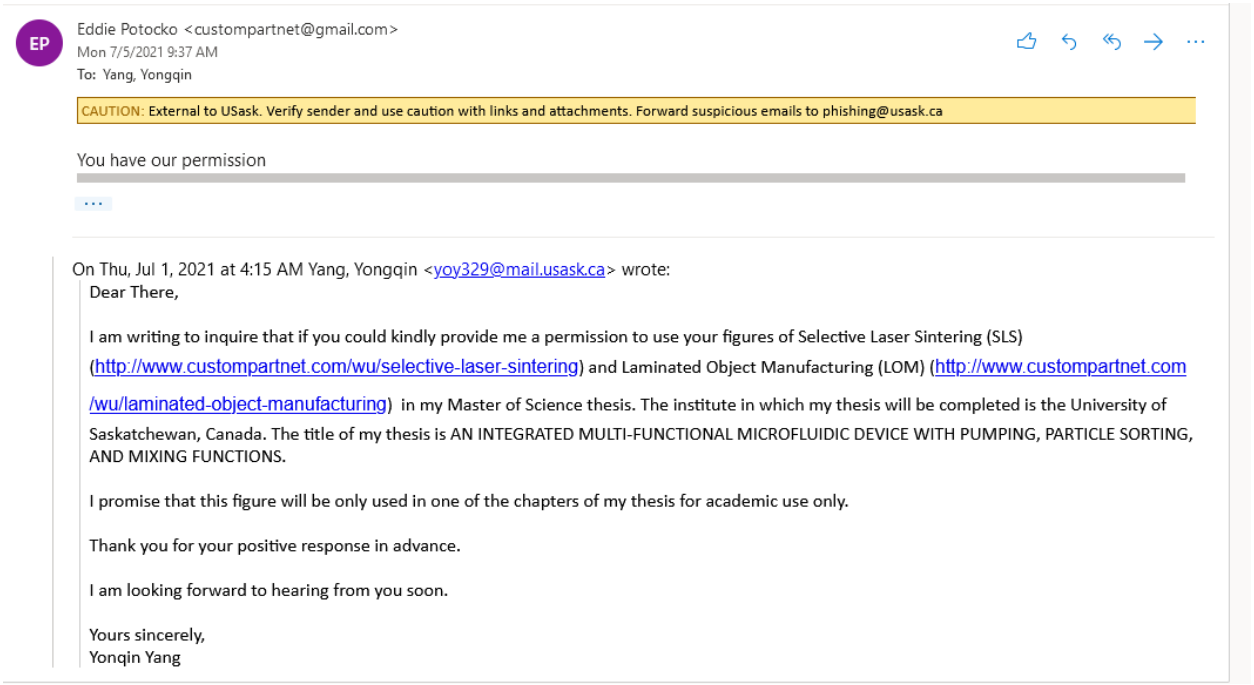

EP

Eddie Potocko <custompartnet@gmail.com>
Mon 7/5/2021 9:37 AM
To: Yang, Yongqin

CAUTION: External to USask. Verify sender and use caution with links and attachments. Forward suspicious emails to phishing@usask.ca

You have our permission

...

On Thu, Jul 1, 2021 at 4:15 AM Yang, Yongqin <yoy329@mail.usask.ca> wrote:

Dear There,

I am writing to inquire that if you could kindly provide me a permission to use your figures of Selective Laser Sintering (SLS) (http://www.custompartnet.com/wu/selective-laser-sintering) and Laminated Object Manufacturing (LOM) (http://www.custompartnet.com/wu/laminated-object-manufacturing) in my Master of Science thesis. The institute in which my thesis will be completed is the University of Saskatchewan, Canada. The title of my thesis is AN INTEGRATED MULTI-FUNCTIONAL MICROFLUIDIC DEVICE WITH PUMPING, PARTICLE SORTING, AND MIXING FUNCTIONS.

I promise that this figure will be only used in one of the chapters of my thesis for academic use only.

Thank you for your positive response in advance.

I am looking forward to hearing from you soon.

Yours sincerely,
Yonqin Yang

B: Mesh in COMSOL

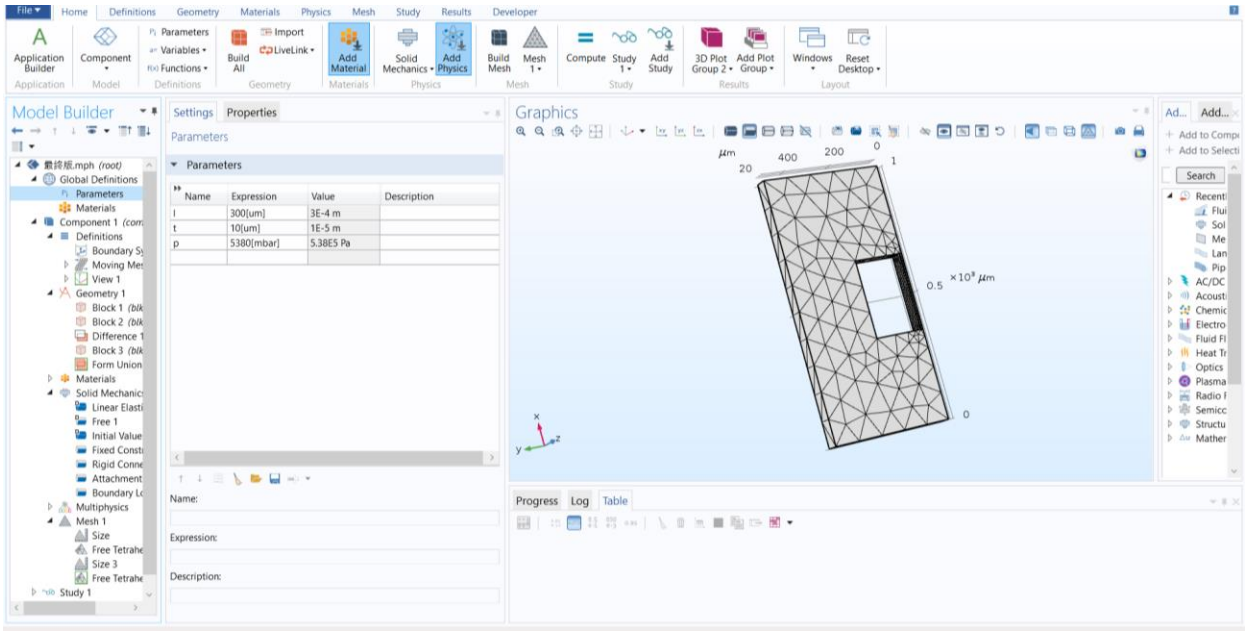

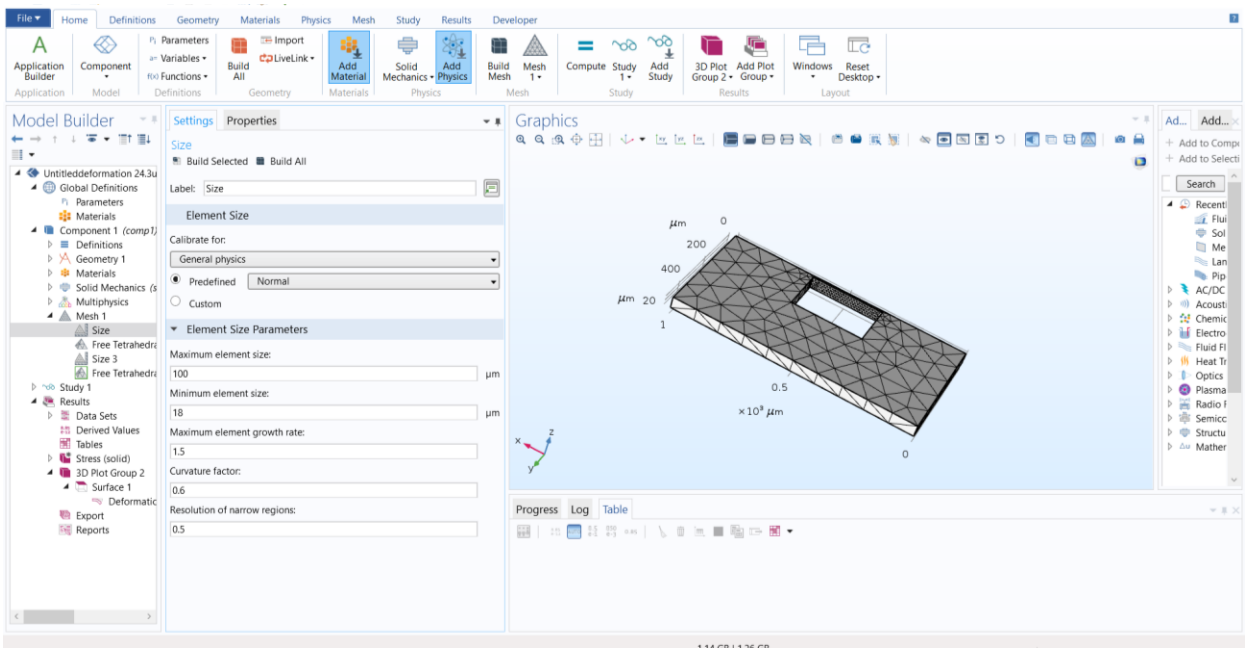

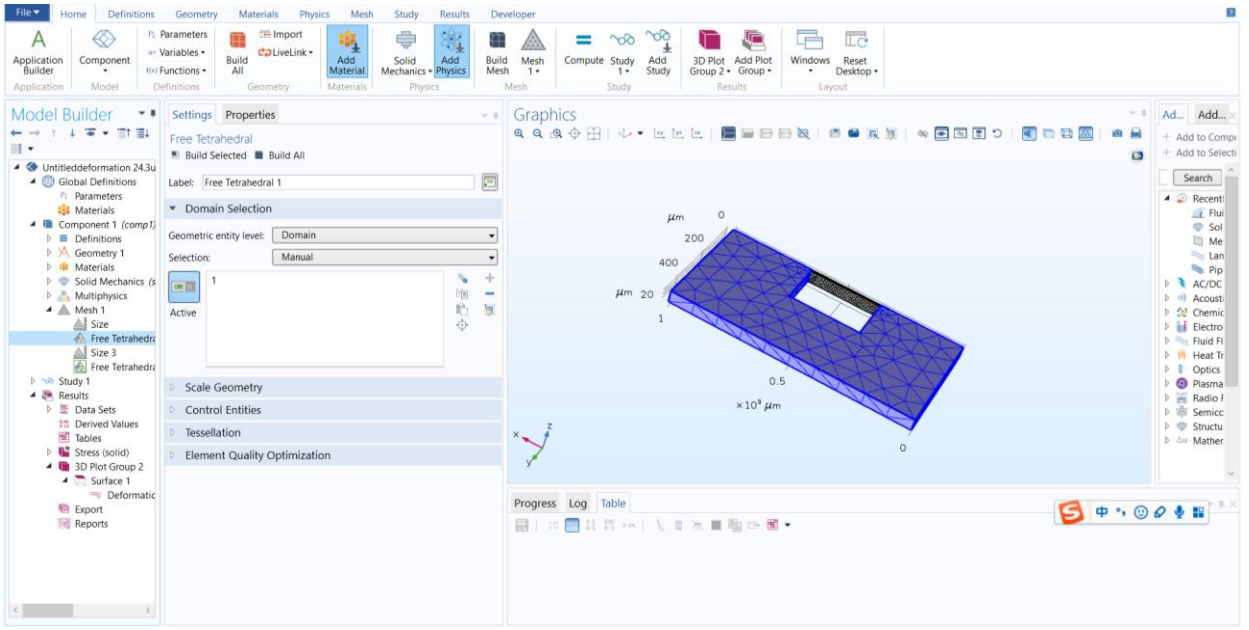
File
Home
Definitions
Geometry
Materials
Physics
Mesh
Study
Results
Developer
Model Builder
Settings
Properties
Free Tetrahedral
Build Selected
Build All
Label: Free Tetrahedral 1
Domain Selection
Geometric entity level: Domain
Selection: Manual
Active
Scale Geometry
Control Entities
Tessellation
Element Quality Optimization
Graphics
Progress
Log
Table

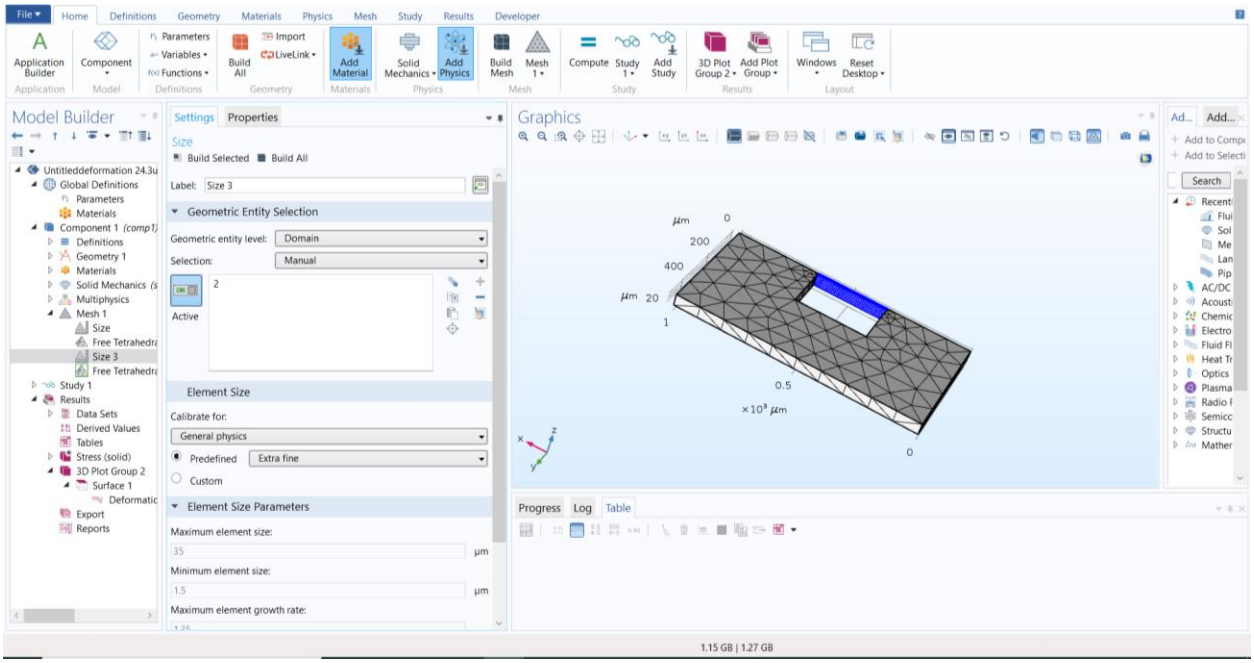
File
Home
Definitions
Geometry
Materials
Physics
Mesh
Study
Results
Developer
Model Builder
Settings
Properties
Size
Build Selected
Build All
Label: Size 3
Geometric Entity Selection
Geometric entity level: Domain
Selection: Manual
Active
Element Size
Calibrate for:
General physics
Predefined
Extra fine
Custom
Element Size Parameters
Maximum element size:
35
μm
Minimum element size:
1.5
μm
Maximum element growth rate:
Graphics
Progress
Log
Table
1.15 GB | 1.27 GB

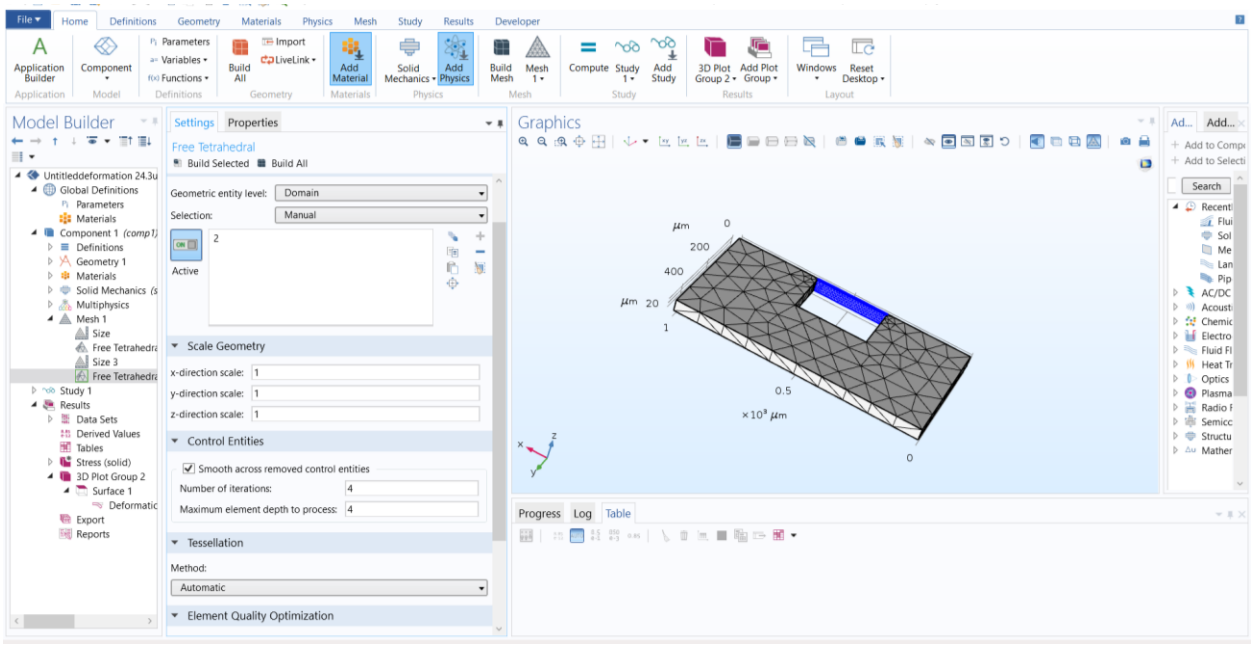
File
Home
Definitions
Geometry
Materials
Physics
Mesh
Study
Results
Developer
Application Builder
Component
Parameters
Variables
Functions
Build All
Import
LiveLink
Add Material
Solid Mechanics
Add Physics
Build Mesh
Mesh 1
Compute
Study 1
Add Study
3D Plot Group 2
Add Plot Group
Windows
Reset Desktop
Model Builder
Settings
Properties
Free Tetrahedral
Build Selected
Build All
Geometric entity level:
Domain
Selection:
Manual
Active
Scale Geometry
x-direction scale:
y-direction scale:
z-direction scale:
Control Entities
Smooth across removed control entities
Number of iterations:
Maximum element depth to process:
Tessellation
Method:
Automatic
Element Quality Optimization
Graphics
Progress
Log
Table
Search